FILE

James Rennell Centre
for Ocean Circulation

INTERNAL DOCUMENT No. 18

Numerical modelling of eddy-driven fluid exchange between the oceanic mixed-layer and thermocline

J W Zhang & A G Nurser

1995

Institute of
Oceanographic Sciences
Deacon Laboratory

Natural Environment Research Council

JAMES RENNELL CENTRE FOR OCEAN CIRCULATION

INTERNAL DOCUMENT No. 18

Numerical modelling of eddy-driven fluid exchange between the oceanic mixed-layer and thermocline

J W Zhang & A G Nurser

1995

Gamma House
Chilworth Research Park
Chilworth
Southampton SO1 7NS
Tel 0703 766184
Telefax 0703 767507

DOCUMENT DATA SHEET

AUTHOR
ZHANG, J W & NURSER, A G

PUBLICATION DATE 1995

TITLE

Numerical modelling of eddy-driven fluid exchange between the oceanic mixed-layer and thermocline.

REFERENCE

James Rennell Centre for Ocean Circulation, Internal Document, No. 18, 18pp. & figs.
(Unpublished manuscript)

ABSTRACT

The role of the eddies in mixing down properties from the mixed-layer into the thermocline is studied using a numerical model of a mixed layer above a mesoscale baroclinically unstable front. Vertical velocities of up to ~50mday-1 develop, which push tongues of a ventilation tracer, initially only present within the surface layer, down to depths of ~120m. Fronts of various strengths are studied.

The horizontally averaged model results are simulated with a one-dimensional diagnostic model which includes wind mixing and vertical diffusive mixing. For a front of similar strength to those observed in the western subtropical Atlantic, the eddy transfer of tracer is well parameterized with an eddy-induced vertical diffusivity of ~6cm2s-1. However the vertical profile of horizontally averaged temperature field does not mix at all; rather it steepens. The stronger the front, the more rapidly and deeply the tracer is spread.

KEYWORDS

BAROCLINIC INSTABILITY
EDDIES
FRONTS
MIXED LAYER
VENTILATION

ISSUING ORGANISATION

Institute of Oceanographic Sciences
Deacon Laboratory
Wormley, Godalming
Surrey GU8 5UB. UK.

Director: Colin Summerhayes DSc

Telephone Wormley (0428) 684141
Telex 858833 OCEANS G.
Facsimile (0428) 683066

Copies of this report are available from: **The Library,** *PRICE* £00.00

Executive Summary

The eddy transport of properties from the mixed-layer into the thermocline is studied in a numerical model of mesoscale (~50km wide) baroclinically unstable fronts in a reentrant channel. A high resolution Cox and Bryan type code, including a simple Kraus-Turner model of the mixed layer, is employed.

Strong vertical circulations develop, associated with the growing instabilities, with local downwelling rates of up to $30 - 90\ mday^{-1}$ These push tongues of a 'ventilation tracer', initially only present within the surface layer, down to depths of about 120 m into the thermocline. For a front similar to those observed in the western subtropical North Atlantic during the FASINEX observations, about half of the ventilation tracer was deposited into the thermocline over a period of 20 days of vigorous eddy activity.

Fronts of various strengths are modelled: the stronger downwelling associated with a stronger front pushes the tracer down more deeply, so depositing more of it into the thermocline.

The full, horizontally averaged, model results are simulated by a one-dimensional diagnostic model with constant diffusivity in order to estimate approximate 'eddy-induced' vertical diffusivities for temperature and ventilation tracer. The vertical profile of horizontally averaged temperature field does not mix at all; rather it steepens, so the diagnostic model cannot predict the temperature field accurately. On the other hand it predicts the ventilation tracer field well, if the 'best fit' tracer diffusivity is employed. For the FASINEX front, the 'best fit' tracer diffusivity was $\sim 6 cm^2 s^{-1}$, almost an order of magnitude greater than the imposed model vertical diffusion of $1 cm^2 s^{-1}$. The stronger the front, the larger the best fit diffusivity for tracer.

Runs without the wind-mixed layer show considerably less downward transfer of the ventilation tracer, with best fit diffusivity of $\sim 1.6 cm^2 s^{-1}$ for the FASINEX front.

1. Introduction

Eddies can play important roles in transporting properties from the mixed-layer to lower layers. They can drive strong vertical circulations, such as the vertical velocities up to 25 $mday^{-1}$, diagnosed (Pollard and Regier 1992) within the frontal regions during the Frontal Air-Sea Interaction Experiment (FASINEX). An analogy (Follows and Marshall, 1994) may be drawn between oceanic mixed-layer/thermocline exchange and atmospheric stratosphere/troposphere exchange, much of which is associated with depressions striking the tropopause.

The FASINEX front discussed by Pollard and Regier is a strong surface-intensified front (Fig. 1a). At the surface the density jump is 0.7 kgm^{-3} over about 25 km, but at 300 m depth the density gradient vanishes (Fig. 1b). The Rossby radius is about 10 km. Surface-intensified eddies developing on the front were observed, with horizontal scales of 40 km and vertical scales of ~200 m.

On the other hand, the weaker fronts observed in the North Atlantic Polar Front had meanders with wavelength about 85 km but much weaker vertical motions, of 5 $mday^{-1}$ (Fiekas et.al. 1994 and Strass 1994).

Considerable effort has already gone into modelling the front studied by Pollard and Regier. Samelson (1993) found that linear instability theory suggested that the front was unstable, and that the fastest growing perturbations had e-folding time scales of 2-3 *days*, and along-front wavelengths near 70 km. This implied eddy scales consistent with those observed. Modelling studies of the dynamics of the same front, (Onken 1992) suggest that downwelling (occurring downstream of the ridges) and upwelling (downstream of the troughs) were driven by geostrophic advection of relative vorticity. Both upwelling and downwelling were as strong as 10 $mday^{-1}$. The wavelength was about 85 km. The peak vertical velocities diagnosed by Pollard and Regier are probably associated with sharpening of the front (frontogenesis), as modelled by (Wang 1993), who found vertical *downwelling* velocities up to 50 to 100 $mday^{-1}$.

Spall (1994 in press) has modelled the subduction, a result of the strong vertical circulation in frontal regions, which occurs when water is pulled down and below the front by the downwelling on the cold side of the front. The modelled downwelling was in the order of 30 $mday^{-1}$ in a frontal case in FASINEX (the same case as Samelson 1993). A total permanent subduction rate driven by frontogenesis was about 20 $myear^{-1}$ between the isopycnal layer 25.7 and 26.0 kgm^{-3} on the warm side of the

front but outside the meander envelope of the front over a 100-day integration. Temporary or local subduction rates were much larger, for example, about 100 to 200 $myear^{-1}$ over the same isopycnal layers but including both warm and cold sides of the front.

A failing of present 1-D models of the mixed-layer is that they ignore the interaction with the mesoscale eddy field variability. We are presently examining how it might be possible to parameterise these eddy-induced exchanges, which will be poorly resolved even by eddy-resolved models.

We are studying eddy interactions by running a regional model of an unstable front. A standard Cox and Bryan type level model is run at high resolution, with a simple Kraus-Turner mixed-layer scheme.

A ventilation tracer is inserted into the mixed-layer at the start of the run. As the front goes unstable, warm waters from the south override the cold northern waters, which slump southward. Stratification is generated, and the mixed-layer shallows. However the vertical velocities associated with the growing instabilities push tongues of tracer down to depths of ~120 m into the thermocline (Fig. 9). These tongues of high tracer concentration are reminiscent of the chlorophyll streamers, penetrating down to depths of 400 m, observed in the Vivaldi cruise (Fig. 2).

In this report, section 2 is the description of the model and initial conditions. The model results are presented in section 3. The relationship between front strength and eddies is discussed in section 4. The role of the mixed-layer scheme is detailed in section 5. In section 6, a one-dimensional diagnostic model is applied to further study the effects of eddies in transporting properties from the mixed-layer into the thermoclines. Channel width is discussed in section 7. Section 8 describes the results when using the Pacanowski-Philander Richardson number dependent mixing scheme; which increases the diffusivity just below the mixed-layer. Section 9 is then the conclusion.

2. The model and initial conditions:

We are studying eddy interactions by running a regional model of an unstable front. The MOMA code is run at high resolution (2km x 2km x 10m), with a simple Kraus-Turner mixed-layer scheme. The QUICK algorithm (Farrow and Stevens 1994) is employed to advect tracers. It produces tracer fields considerably smoother than the standard advection scheme. No slip conditions are applied on both south and north boundaries (cross-front), with periodic conditions on east and west boundaries (along-front).

The first run is called Case A, other cases are listed in Table 1 and will be discussed later. The central band (50 *km* wide) of Case A is initialised with a mesoscale front from Samelson 1993 (Fig. 3), an idealisation of Pollard and Regier's FASINEX front. The cross-front temperature difference is about 2.8 $^{\circ}C$ near the surface. The initial state is zonally uniform (along-front), while meridionally, the central part is more stratified. The Rossby radius is about 10 *km* in Case A, with a theoretical e-folding growth scale for the fastest growing instabilities of 2 to 3 *days*. A geostrophic jet is imposed. An initial perturbation is imposed in the central stratified area in the form of

$$T(x,y,z) = zT_{\max}\sum_{i=1}^{7} c_n \sin(\frac{2\pi L}{\lambda}\frac{x}{L})\exp(-16(y-0.5)^2)$$

with c_n is a random number between 0 and 1; z is 1 at the surface and 0 at the bottom; T_{max} is in the order of 0.01 $^{\circ}C$; L is the length of the channel; λ_n is wavelength (2, 3, 5,7, 10, 20 and 25 *km*). In addition, perturbation to the velocity field is imposed to make sure the flow remains geostrophic.

A ventilation tracer is introduced in a way that, initially it has a value 1.0 within the mixed-layer (depth of 10 *m*) and 0.0 otherwise.

In order to work against the stratification and deepen the mixed-layer, the model is forced with a uniform turbulent kinetic energy input of $10^{-3} Wm^{-2}$; this is the same energy as would be implanted by a uniform wind stress of 0.1 Nm^{-2}. No momentum is added, so the forcing does not speed up the jet.

The horizontal viscosity is 50 $m\ s^{-1}$, diffusivity is 10 $m\ s^{-1}$. The vertical viscosity is 5 $cm\ s^{-1}$, diffusivity is 1 $cm\ s^{-1}$except mentioned otherwise.

3. Case A

The instability develops as time increases. At day 28, the wavelength of the most unstable wave is about 80 *km* (Fig. 4). Warm water is transported northward, while cold water southward.

The vertical velocity at the same time at depth 30 *m* indicates downwelling in troughs and upwelling in crests (Fig. 5), consistent with the release of available potential energy. The maximum of downwelling is in the order of 47 $m\ day^{-1}$ associated with frontogenesis along the warm front, while 17 $m\ day^{-1}$ for upwelling (stronger vertical motions than Onken 1992, similar order to Wang 1993). At day 35, the downwelling increases to 66 $m\ day^{-1}$, while upwelling 21 $m\ day^{-1}$ (Table 2).

The surface tracer field at day 28 shows the same tendency as temperature: wavelength is also about 80 *km* (Fig. 6). The tracer has lower value within the deeper mixed-layer (less stratified) areas as it is mixed further down in these areas (Fig. 7). On the other hand, the tracer at depth 55 *m* (Fig. 8) is higher within the mixed-layer areas.

The along-front section of tracer in the central stratified area (Fig. 9) shows that the tracer has been pushed from the mixed-layer to lower layer. The temperature structure at the same section (Fig. 10) is different from the tracer. Therefore, the tracer is not just pushed into the isotherms.

The zonal mean of tracer at day 21, 28 and 35 (Fig. 11) indicates that, the tracer is pushed down to lower layers as the instability develops. The contour of 0.02 reaches 100 *m* at day 21, nearly 140 *m* at day 28 and 160 *m* at day 35, considerably deeper than the mixed-layer which is nowhere deeper than 80 *m* (Fig. 7).

The horizontal means of the tracer at day 7, 14, 21, 28 and 35 (Fig. 12) illustrate that, as the instability develops, the value of tracer in the upper part of the ocean (60 *m*) decreases, while below 60 *m* it increases. The tracer is pushed down as deep as 175 *m* at day 35.

The horizontal means of temperature at the same days (Fig. 13) differ from these of the tracer. At the early stage of the growth of instabilities, the temperature decreases in the upper part of the basin (day 7, 14 and 21) as the mixed-layer deepens. Later on, the mixed-layer shallows and the *average* surface temperature increases as warm water slumps upward and northward. Deeper down, the temperature slightly decreases as cold water slumps south, available potential energy is lost and the isotherm at the front becomes less steep.

In summary, the instabilities on the fronts have wavelength of 80 *km*. Strong vertical circulation is diagnosed: at day 35, the maximum of downwelling is up to 66 $m\ day^{-1}$ and upwelling 21 $m\ day^{-1}$ (Table 2). The tracer is pushed down as deep as 175 *m* at day 35 (Fig. 12). Zonal mean

isotherms slump (Fig. 14), becoming less steep as the instabilities develop and extract available potential energy.

4. Front strength

In order to study the effect of frontal instability on tracer transport, Case B (with the strongest front) and Case C (with the weakest front) are compared with Case A (Tables 1 and 2). The initial perturbation in Cases B and C is the same as in Case A.

4.1 Case B (the strongest front)

Compared with Case A, the instability develops more quickly in Case B though the same initial perturbation is imposed. At day 21, temperature at depth 5 *m* (Fig. 15) has a wavelength of about 120 *km* (it was 80 *km* at day 28 in Case A).

Meanwhile, the zonal mean of tracer at day 21 (Fig. 16) indicates that, the tracer is pushed down as deep as near 180 *m* (it was 160 *m* at day 35 in Case A). Thus, the tracer is transported deeper with stronger front. This conclusion is supported by the basin mean of tracer in Case A and Case B (Fig. 17). In Case A, the maximum depth of tracer is about 175 *m* at day 35, while in Case B 185 *m* at day 21.

4.2 Case C (the weakest front case)

The initial front in Case C is half the strength of the one in Case A. The instability develops more slowly than in Case A. At day 56, the wavelength is about 75 *km* (Fig. 19). The zonal mean of tracer at day 28, 42 and 56 (Fig. 21) illustrates that the tracer is pushed downward as the instability develops. At day 56, the tracer is transported to less than 140 *m* (it was 160 *m* in Case A and 180 *m* in Case B). The basin mean of the tracer at day 28, 42 and 56 (Fig. 18) shows similar tendency: the mixed-layer shallowed as the instability develops, the value of tracer above 80 *m* decreases (as a result of mixing), while between 80 *m* to 170 *m* depth, the value of tracer increases. Note that the mixed-layer is deeper in this run than in the previous Cases A and B since the slower development of the instability has allowed the more time for wind mixing.

4.3 Front strength and potential energy

The evolution of the basin-integrated potential energy for Cases A to C is shown in Fig. 22. Initially the potential energy rises in all cases as a consequence of the wind energy being fed into the mixed layer model and the vertical background diffusive mixing of temperature. However, after a time, the instabilities start to grow rapidly, transforming potential energy into kinetic energy, as the isotherms slump. The stronger the front, the larger the 'available potential energy' — the amount of potential energy released as the isotherms slump. With

the weak front, Case C, the eddies consume available potential energy more slowly than potential energy is fed in through the wind mixing and vertical diffusive mixing, so total potential energy rises throughout the integration, while with the stronger fronts B and C more available potential energy is consumed by the eddies, and total potential energy falls as the isotherms slump.

4.4 Subduction Rates

Fig. 23 shows the time evolution of the tracer load which penetrates into the thermocline, expressed as a percentage of the total load. The stronger the front, the larger and more vigorous the instabilities, and the greater the deposition of tracer into the thermocline (eg. ~42% at day 35 in Case A; ~45% at day 21 in Case B, the strongest front and 33% at day 56 in Case C, the weakest front). Direct conversion of the tracer deposition rate into a subduction rate, defined as a the rate at which mixed-layer fluid is transferred into the thermocline, is difficult. Indeed the usefulness of the term 'subduction rate' is uncertain in a situation like that modelled here, where there is more exchange of fluid between than systematic transfer of fluid from mixed-layer to thermocline. Tracers whose values in the mixed layer are reset on different time scales will pass into the thermocline at different rates.

However let us assume that at the start of vigorous instability, the average tracer concentration in the mixed-layer is C_{mix}, which varies, depending on the run, from ~0.1-0.13, according to how much the mixed layer has deepened. Assuming that later variations in the tracer concentration within the mixed-layer are comparatively small, the fluid transfer into the thermocline may be estimated as

$$\frac{\text{increase in thermocline tracer load}}{C_{mix}}$$

This gives average subduction rates of 435 $myear^{-1}$ (~1.19 $mday^{-1}$) between day 21 to 35 for Case A, 1048 $myear^{-1}$ (~2.87 $mday^{-1}$) between day 14 to 21 for Case B, and 208 $myear^{-1}$ (~0.57 $mday^{-1}$) between day 28 to 56 for Case C.

In summary, the stronger the front, the more the available potential energy, the more quickly the instability develops and the longer the wavelength. The ventilation tracer is pushed deeper by the stronger fronts. The stronger the front, the greater the subduction rate.

5. Effect of the Kraus-Turner mixed-layer scheme

Cases A, B and C are with the Kraus-Turner mixed-layer scheme using the same input of turbulent energy to work against the stratification. In order to study the effect of surface forcing on tracer

transport, Case D is run without the Kraus-Turner mixed-layer scheme (no forcing), but with the same front strength and initial conditions as Case A.

In Case D, the instability develops with similar time scale and wavelength (Fig. 23) as to Case A. The tracer (Fig. 24) is also pushed downward and across the front as the instability develops. Especially, at day 35, a tongue extends as deep as 130 m. The basin mean of tracer (Fig. 25) shows the same tendency. Since there is no mixed-layer scheme, the tracer in Case D is not transported as deep as in Case A: 155 m in Case D and 175 m in Case A at day 35.

Similar to Case A, the basin mean temperature of Case D (Fig. 26), at the early stage of growth, slightly decreases in the upper part of the domain. Later on, the basin mean surface temperature increases as warm water slumps upward and northward. Deeper down, the temperature slightly decreases as cold water slumps south.

Thus, without the mixed-layer scheme, the tracer is not transported as deep as in the case with the scheme. However, the instability developed in similar time scale and wavelength in both cases with and without the mixed-layer scheme: in both Cases A and D, the wavelength is about 80 km, the maximum growth is between day 21 to 35.

6. A one-dimensional diagnostic model

In order to model the effects of eddies on transporting the tracer from mixed-layer to thermocline, a one-dimensional diagnostic model is applied:

$$\frac{\partial C_k}{\partial t} = k_v \frac{\partial^2 C_k}{\partial z^2}$$

with C_k is the value of temperature or tracer. k_v is the vertical diffusivity.

In addition, the same mixed-layer scheme is included. The forcing is controlled by the forcing factor m: m is the ratio of forcing to the actual forcing. m of 0.0, for example, means there is no wind energy forcing, while m of 1.0 means the wind energy forcing is the same as in the actual model ($10^{-3} Wm^{-2}$).

This diagnostic model is initialised with the horizontal mean temperature or tracer at a chosen time t_0(e.g. $t_0$is day 21 in Case A) and then run to time t_1 (t_1 is day 35, for example, in Case A) (Table 3). Two types of mean are applied: whole-channel mean and central mean (between latitude 30.1 to 30.3° N) of temperature/tracer.

A normalised mean squared error, $\langle s^2 \rangle$, is used to examine how well the diagnosed temperature/tracer fits the actual value:

$$\langle s^2 \rangle = \int_{t_0}^{t_1} \int_{z=0}^{z=300m} (C_k - C_A)^2 \Big/ \int_{t_0}^{t_1} \int_{z=0}^{z=300m} (C_A - C_{A_{t_0}})^2$$

with C_k is the temperature/tracer in the diagnostic model, C_A is the "real" value of temperature/tracer. Both C_k and C_A are functions of time and depth. $C_{A_{t_0}}$ is the C_A at time t_0. The smaller the $\langle s^2 \rangle$, the better the fit of the C_k to actual value C_A. If $\langle s^2 \rangle$ equals zero, then the diagnosed C_k has the same value as the C_A in the actual model. $\langle s^2 \rangle$ equals or larger than one means the "model" value of temperature/tracer is a poor approximation to the "real" value. Thus only if $\langle s^2 \rangle$ is smaller than one can the diffusive model be considered useful.

We first attempt to predict the whole-channel mean of temperature with the diagnostic model. Fig. 27 illustrated the variation of $\langle s^2 \rangle$ with vertical diffusivity k_v. The error function $\langle s^2 \rangle$ is near or above one, i.e., the diagnostic model gives a poor approximation of temperature to the "real" value. The best fit diffusivities k_v (with minimum $\langle s^2 \rangle$) of Cases A to C are listed in Table 4. In all three kinds of initial front strength, the best approximated k_v for temperature is with forcing factor m = 0 (i.e.. there is no wind energy forcing in the diagnostic model). The weaker the front, the better the estimated C_k to the "actual" value C_A.

The best fit diffusivity k_v for the central mean of temperature is higher than the one for the whole-channel mean (Table 4). Also, the minimum of $\langle s^2 \rangle$ is smaller than the one for the whole-channel mean. However, $\langle s^2 \rangle$ is still about or higher than one (except in Case C), that is, the diagnostic model predicts the temperature field poorly.

On the other hand, the diagnostic model gives much better results for the tracer field. For the whole-channel mean of tracer in Case A, quite low values of $\langle s^2 \rangle$ (0.1 to 0.2) are obtained with values of k_v about 5.0 $cm^2 s^{-1}$ (Fig. 28). The best fit vertical diffusivity k_v for tracer is higher than the one for temperature: e.g. in Case A, the best fit k_v for tracer is about 5.2 $cm^2 s^{-1}$ while for temperature is 1.2 $cm^2 s^{-1}$ (Figs. 27 and 28). Similar to the diffusivities for temperature, the weaker the front (Table 4), the better fit of the diagnostic model, and the smaller the k_v. For the whole-channel mean, minimum $\langle s^2 \rangle$=0.05 was obtained with k_v=1.6 $cm^2 s^{-1}$ for the weakest front, Case C, whereas minimum $\langle s^2 \rangle$=0.12 was obtained with k_v=8.8 $cm^2 s^{-1}$ for the strongest front, Case B.

For the central mean of tracer of Case A, the best fit diffusivity is larger than the one for the whole-channel mean (Figs. 28 and 29). This conclusion is also true for the weakest front Case C (Table 4). But in Case B (the strongest front) k_v for the central mean (8.6 $cm^2\ s^{-1}$) is smaller than the one for the whole-channel mean (8.8 $cm^2\ s^{-1}$). In all these three cases, $\langle s^2 \rangle$ for the central mean is larger than the one for the whole-channel mean. Thus, the diffusive model of vertical tracer transfer for the whole-channel mean gives better results.

Finally, in Cases A to C, the best fit diffusivity (with minimum $\langle s^2 \rangle$) for tracer is higher than the one for temperature, for both the whole-channel mean and the central mean (Table 4).

Not surprisingly, in Case D (without the Kraus-Turner mixed-layer scheme), the minimum of $\langle s^2 \rangle$ is with forcing factor m of 0 (Fig. 30). In the case of the whole-channel mean, the diagnostic model with the best fit vertical diffusivity gives a poor approximation to the actual temperature. But the vertical diffusivity for tracer (Fig. 31) gives better results. The best fit diffusivity for temperature/tracer for both the whole-channel mean and the central mean in Case D (without the Kraus-Turner mixed-layer scheme) is smaller than the one in Case A (with the mixed-layer scheme) (Table 4).

In summary, the one-dimensional diffusive diagnostic model gives temperatures which are poor approximations to the actual values. But it generally predicts the tracer distribution fairly well. This holds

both for the whole-channel mean and the central mean. For the cases of the whole-channel mean, the stronger the front, the larger the k_v for tracer, but the smaller the mixed-layer energy gain m. For the cases of the central mean of tracer, the diffusive model does not give as good results as it does for the whole-channel mean. In all four cases (Cases A to D), the weaker the front, the better the fit (the smaller $\langle s^2 \rangle$) of the temperature and tracer fields predicted by the diffusive diagnostic model.

7. Channel width

In order to examine whether the current channel is wide enough to avoid problems caused by the north and south solid walls, Case E is designed with the same length and depth of Case A, but double the width of Case A. The same initial conditions and perturbations as Case A are imposed in the central area of Case E, while meridionally uniform temperatures are specified near both the south and north of the boundaries.

Similarly to Case A, the instability develops as time increases. The most active period is between day 21 to 35 (the same as in Case A). At day 28, fronts develop with wavelength about 80 *km* (Fig. 32). At day 35, the maximum of upwelling and downwelling are in the same order as in Case A (Table 2).

The zonal mean of tracer e.g. at day 35 in Case E (Fig. 33) and Case A (Fig. 11c) are very similar, it thus suggests that the channel in Case A is wide enough to avoid problems caused by the north and south solid walls.

The channel width in Case A hence appears to be sufficient for the current simulations.

8. The Pacanowski-Philander scheme for vertical viscosity and diffusivity

In all the cases above (Cases A to E), constant vertical viscosity and diffusivity have been used. In the following Case F, the Pacanowski-Philander scheme for vertical viscosity and diffusivity is applied. The Pacanowski-Philander scheme is generally thought to be a good scheme for the tropics, though it is applied to the frontal case in mid-latitude here.

According to Pacanowski and Philander (1981),

viscosity $\nu = \frac{\nu_0}{(1+\alpha R_i)^n} + \nu_b$

and diffusivity $\kappa = \frac{\nu}{(1+\alpha R_i)} + \kappa_b,,$

with ν_0 is an adjustable parameter (150.0 $cm^2 s^{-1}$); ν_b is the background viscosity (10 $cm^2 s^{-1}$); κ_b is the background diffusivity (1 $cm^2 s^{-1}$); α is 5; R_i is Richardson number, n is 2 (Fig. 34). Both viscosity and diffusivity are limited with a minimum of 10 $cm^2 s^{-1}$ near the surface and a maximum of 50 $cm^2 s^{-1}$ in other layers.

The same initial conditions and perturbation as Case A are imposed in Case F. At day 28, the wavelength of the instabilities (~80 km) (Fig. 35) is similar to the one in Case A. The depth of the mixed-layer at day 28 (Fig. 36) shows similar wavelength (~80 km) and maximum depth (~90 m) as in Case A but has a minimum depth of 20 m (it was 10.5 m in Case A). The difference of the mixed-layer depth in Cases F and A is due to the stronger mixing of horizontal velocity within the mixed-layer, and weaker vertical velocities (see below).

The vertical velocity at depth 30 m at the same time (Fig. 37) shows the maximum downwelling is about 33 $m\ day^{-1}$ (47 $m\ day^{-1}$ in Case A), while upwelling 10.5 $m\ day^{-1}$(17 $m\ day^{-1}$ in Case A). At day 35, the vertical circulation in Case F (Table 2) is also weaker than in Case A.

As a result of weaker vertical circulation in Case F, the zonal mean of tracer during day 21 to 35 (Fig. 38) is transported down about 5 to 10 m less deep in Case F than in Case A. The different magnitude of zonal mean tracer in Case F from Case A is due to the slight difference of the mixed-layer depth between Case F and Case A.

Even though the vertical diffusivity is larger near the surface (~10 $cm^2 s^{-1}$ at depth 5 m) due to the Pacanowski-Philander scheme in Case F, the basin mean tracer (Fig. 39) is transported to the similar depth to Case A: at day 35 the tracer is pushed down to about 175 m in both Case F and Case A.

The basin mean of temperature in Case F (Fig. 40) is similar to the one in Case A. Thus, the overall effect of higher diffusivity and viscosity on temperature in Case F is negligible.

Thus, fronts simulated with the Pacanowski-Philander scheme had similar characteristic to those in Case A (with constant vertical viscosity and diffusivity). Although the vertical circulation was slightly weaker than that in Case A, the tracer was pushed down to a similar depth in both Cases F and A.

9. Conclusions

We have modelled the development of disturbances on small-scale, baroclinically unstable, fronts similar to the front observed in FASINEX which was discussed by Pollard and Regier. The vertical circulations associated with the growing instabilities were found to push tongues of a 'ventilation tracer, initially only present within the surface layer, down to depths of about 120 m into the thermocline. The fraction of the ventilation tracer deposited into the thermocline was found to be substantial, about 40% for Case A after 35 days.

The strength of the fronts determined the wavelength and rate of growth of the instabilities, together with the maximum depth to which the tracer was transported (Table 2). The stronger the front, the more quickly the instability developed and the larger its wavelength. In addition, the stronger downwelling associated with a stronger front pushed the tracer down deeper, so depositing a greater quantity of it into the thermocline.

The Kraus-Turner mixed-layer scheme and eddies colluded to produce deeper mixing than with either separately.

The inclusion of Pacanowski and Philander's Richardson-number dependent vertical mixing scheme has negligible effects on tracer transport and temperature structure.

The time evolution of the horizontally averaged tracer fields has been simulated by a one-dimensional diagnostic model with constant diffusivity. Approximate 'eddy-induced' diffusivities for temperature and tracer have been determined.

(1) The diffusivity in the diagnostic model which gives the best fit to the temperature field of the full model is smaller than the one which gives the best fit for the tracer. The diagnostic model predicts the temperature poorly, but gives good estimates of the actual tracer field.

(2) The best fit diffusivities for both temperature and tracer depend on front strength. The best fit tracer diffusivities increase with the strength of the front from 1.6 $cm^2 s^{-1}$ for the weak front, Case C,

little different to the imposed vertical diffusivity of 1 cm^2s^{-1} to 8.8 cm^2s^{-1} for the strongest front, Case B.

References

Farrow,D.E. and Stevens,D.P. (1994) Tracer advection schemes in ocean general circulation models.

Follows,M.J. & Marshall,J.C. (1994) Eddy driven exchange at ocean fronts. *Ocean Modelling,102,5-9*

Fiekas,V., Leach,H., Mirbach,K-J and Woods,J.D. (1994) Mesoscale instability and upwelling. part 1: observations at the North Atlantic intergyre front. *J.Phys.Oceanogr.,24,1750-1758*

Onken,R. (1992) Mesoscale upwelling and density fine structure in the seasonal thermocline–a dynamical model. *J.Phys.Oceanogr.,22,1257-1273*

Pacanowski,P.C. and Philander,S.G.H. (1981) Parameterization of vertical mixing in numerical models of tropical oceans. *J.Phys.Oceanogr.,11,1443-1451*

Pollard,R.T. and Regier,L.A. (1992) Vorticity and vertical circulation at an ocean front. *J.Phys.Oceanogr.,22,609-625*

Samelson,R.M. (1993) Linear instability of a mixed-layer front. *J.Geophys.Res.,98,10195-10204*

Strass,V.H. (1994) Mesoscale instability and upwelling. Part 2: testing the diagnostics of vertical motion with a three-dimensional ocean front model. *J.Phys.Oceanogr.,24,1759-1767*

Spall,M.A. (in press) Frontogenesis, subduction, and cross-front exchange at upper ocean fronts. *J.Geophys.Res.*

Wang,D-P (1993) Model of frontogenesis: subduction and upwelling. *J.Marine Res.,51,497-513*

Fig. 18. Basin mean of tracer at day 28, 42 and 56 of Case C.

Fig. 19 Temperature at depth 5 m at day 56 of Case C.

Fig. 20 Temperature at depth 5 m at day 28 of Case D.

Fig. 21. Zonal mean of tracer at day 28, 42 and 56 of Case C.

Fig. 22. Potential energy of Cases A to C. The potential energy is scaled by subtracting its initial value.

Fig. 23. Percentage of tracer below the mixed-layer in Cases A to C.

Fig. 24 Zonal mean of tracer at day 21, 28 and 35 of Case D.

Fig. 25 Basin mean of tracer at day 21, 28 and 35 of Case D.

Fig. 26 Basin mean of temperature at day 21, 28 and 35 of Case D.

Fig. 27 Vertical diffusivities (k_v) for temperature with error function $< s^2 >$ of Case A for the case of the whole-channel mean.

Fig. 28 Vertical diffusivity (k_v) for tracer with error function $< s^2 >$ of Case A for the case of whole-channel mean.

Fig. 29 Vertical diffusivity (k_v) for tracer with error function $< s^2 >$of Case A for the case of central mean.

Fig. 30 Vertical diffusivity (k_v) for temperature with error function $< s^2 >$ of Case D for the cases of whole-channel mean and central mean.

Fig. 31 Vertical diffusivity (k_v) for tracer with error function $< s^2 >$ of Case D for the cases of whole-channel mean and central mean.

Fig. 32 Temperature at depth 5 m at day 28 of Case E.

Fig. 33 Zonal mean of tracer at day 35 of Case E.

Fig. 34. The dependence of ν on Richardson number R_i for different cases. We use curve F which is $\nu_0 = 150\ cm^2 s^{-1}$, n = 2 and $\alpha = 5$ (Pacanowski and Philander 1981).

Fig. 35 Temperature at depth 5 m at day 28 of Case F.

Fig. 36 Depth of the mixed-layer at day 28 of Case F.

Fig. 37 Vertical velocity w at depth 30 m at day 28 of Case F.

Fig. 38 Zonal mean of tracer of Case F. (a) day 21, (b) day 28 and (c) day 35.

Fig. 39 Basin mean of tracer at day 7, 14, 21, 28 and 35 of Case F.

Fig. 40 Basin mean of temperature at day 7, 14, 21, 28 and 35 of Case F.

Table 1. List of runs.

Name	Front strength (ΔT at surface) (C)	Kraus-Turner mixed-layer scheme	Pacanowski-Philander scheme	Vertical diffusivity ($cm^2 s^{-1}$)	Channel width (km)
Case A	2.8	Yes	No	1.0	157
Case B	5.6	Yes	No	1.0	157
Case C	1.4	Yes	No	1.0	157
Case D	2.8	No	No	1.0	157
Case E	2.8	Yes	No	1.0	315
Case F	2.8	Yes	Yes	*(a)*	157

(a) with the Pacanowski-Philander scheme.

Table 2. Summary of Cases A to E.

	ΔT (°C)	Time step (s)	Most active period ap	Wave length during ap (km)	Maximum depth of basin-mean tracer at the end of ap (m)	Maximum downwelling ($mday^{-1}$)	Maximum upwelling ($mday^{-1}$)
Case A	2.8	600	day 21 - 35	80	175	66 *(1a)*	21 *(1b)*
Case B	5.6	300	day 14 - 21	120	185	88 *(2a)*	55 *(2b)*
Case C	1.4	1200	day 28 - 56	75	155	32 *(3a)*	16 *(3b)*
Case D	2.8	600	day 21 - 35	80	155	32 *(4a)*	19 *(4b)*
Case E	2.8	600	day 21 - 35	80	175	62 *(5a)*	20 *(5b)*
Case F	2.8	600	day 21 - 35	80	175	35 *(6a)*	20 *(6b)*

ΔT Initial cross-front temperature difference at depth 5 m. *(1a)*. day 35 depth 20 m; *(1b)*. day 35 depth 60 m. *(2a)*. day 21 depth 20 m; *(2b)*. day 21 depth 10 and 20 m. *(3a)*. day 56 depth 30 m; *(3b)*. day 56 depth 40 m. *(4a)*. day 35 depth 20 m.; *(4b)*. day 35 depth 60 m. *(5a)*. day 35 depth 30 m; *(5b)*. day 35 depth 60 m. *(6a)*. day 35 depth 20 m; *(6b)*. day 35 depth 60 m.

Table 3. List of t_0 and t_1

	t_0	t_1
Case A and Case D	day 21	day 35
Case B	day 14	day 21
Case C	day 28	day 56

Table 4. Best fit vertical diffusivity for temperature and tracer.

	The whole-channel mean						The central mean					
	Temperature			Tracer			Temperature			Tracer		
	k_v	$\langle s^2 \rangle$	m	k_v	$\langle s^2 \rangle$	m	k_v	$\langle s^2 \rangle$	m	k_v	$\langle s^2 \rangle$	m
Case A	1.2	0.911	0.0	5.2	0.105	0.25	3.2	0.815 (0.819)	0.0 (0.125)	7.8	0.147	0.25
Case B	0.2	1.002	0.0	8.8	0.121	0.0	1.4	0.848	0.0	8.6	0.364	0.25
Case C	0.6	0.366	0.0	1.6	0.051	0.25	2.0	0.163	0.125	2.6	0.056	0.25
Case D	0.2	1.003	0.0	1.6	0.111	0.0	1.8	0.925	0.0	1.4	0.279	0.0

(k_v is the best fit vertical diffusivity (with minimum $\langle s^2 \rangle$).

$$\langle s^2 \rangle = \int_{t_0}^{t_1}\int_{z=0}^{z=300m} (C_k - C_A)^2 \Big/ \int_{t_0}^{t_1}\int_{z=0}^{z=300m} (C_A - C_{A_{t_0}})^2$$

with C_k is the temperature/tracer in the diagnostic model, C_A is the temperature/tracer in the model (e.g. Case A), t_0 is the starting time for the diagnostic model (e.g. day 21), t_1 is the end time for the diagnostic model (e.g. day 35). m is the forcing factor.

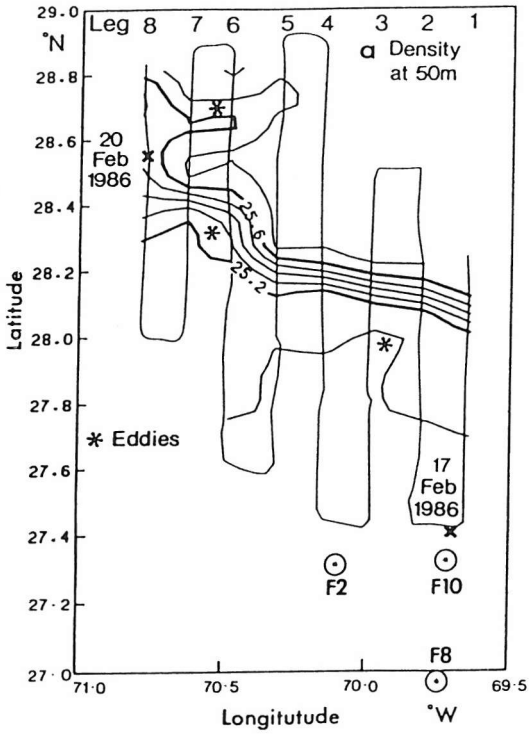

Fig. 1a

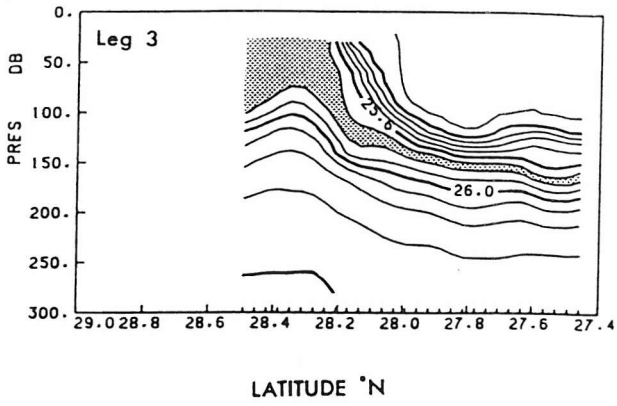

Fig. 1b

Fig. 2

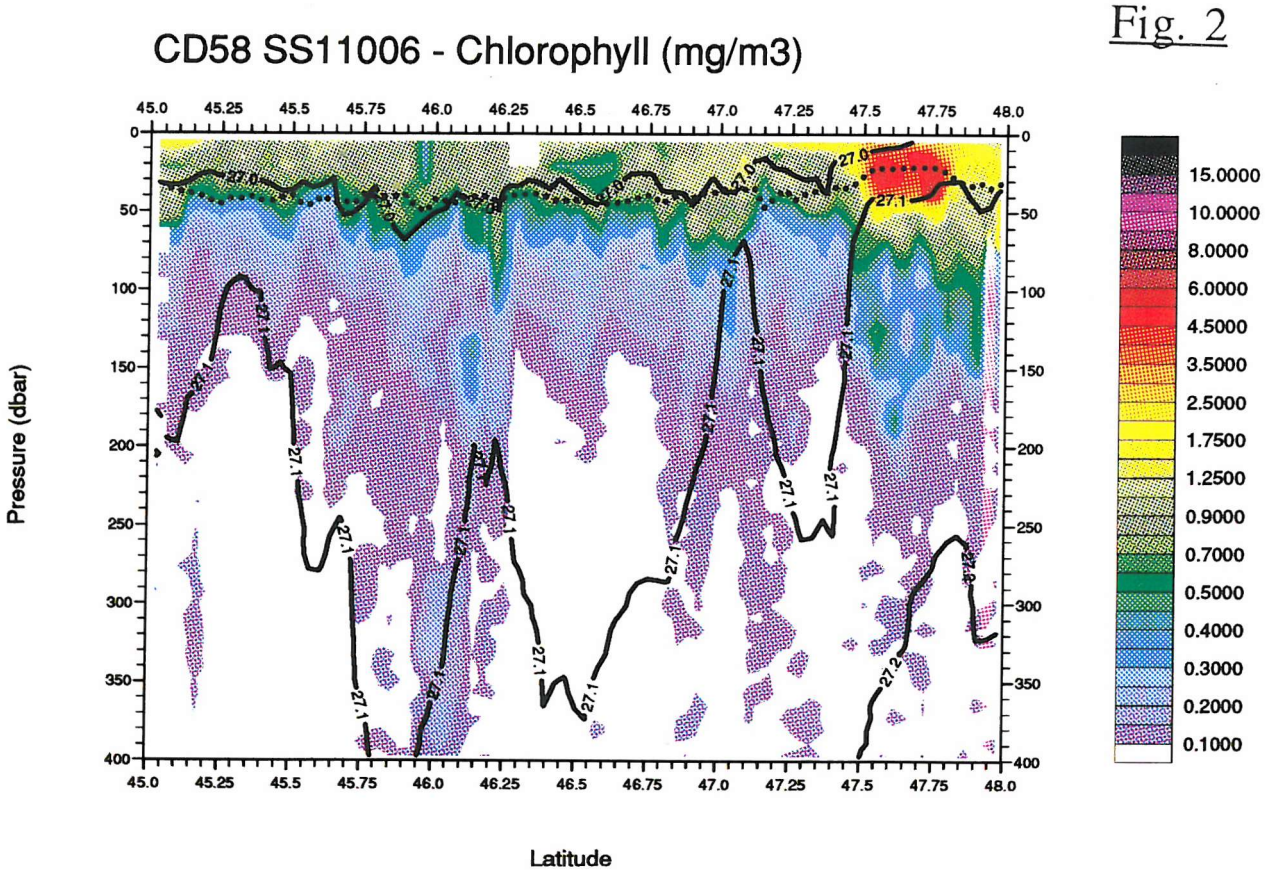

1% PAR level derived from chlorophyll profiles

Temperature , C.I = 0.30, min = 12.90 , max = 20.10 Fig. 3

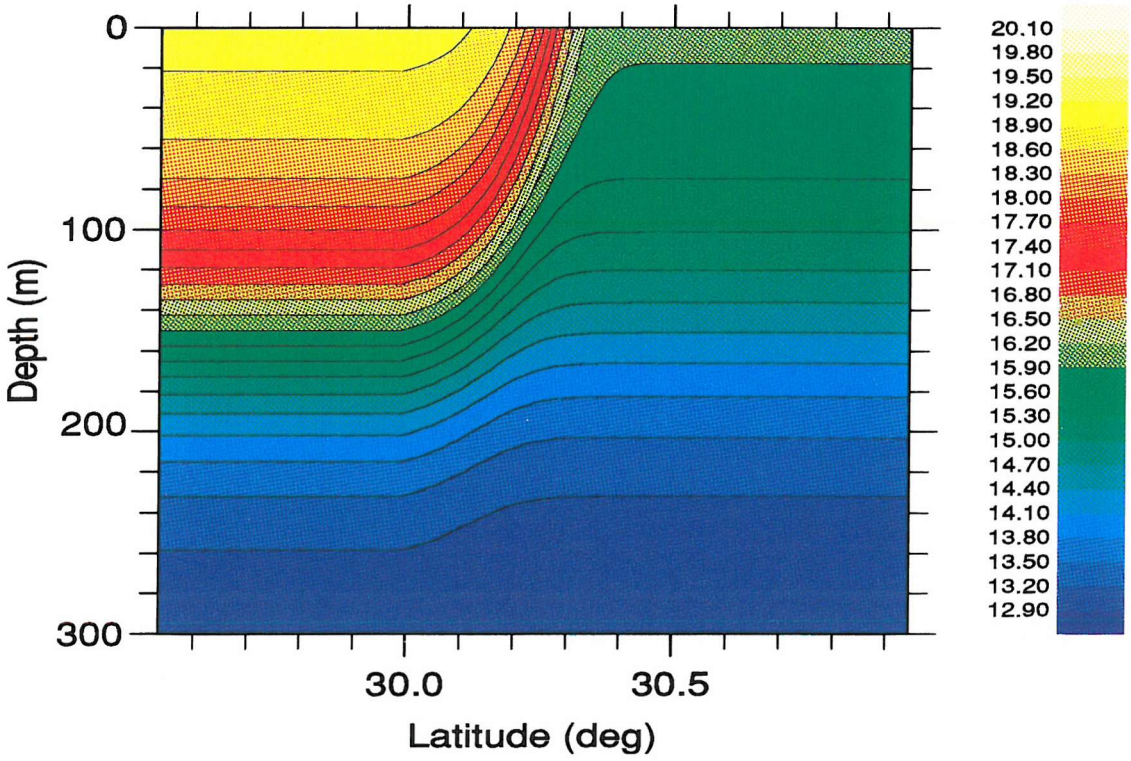

Temperature at depth 5m , min = 12.90, max = 20.10 Fig. 4

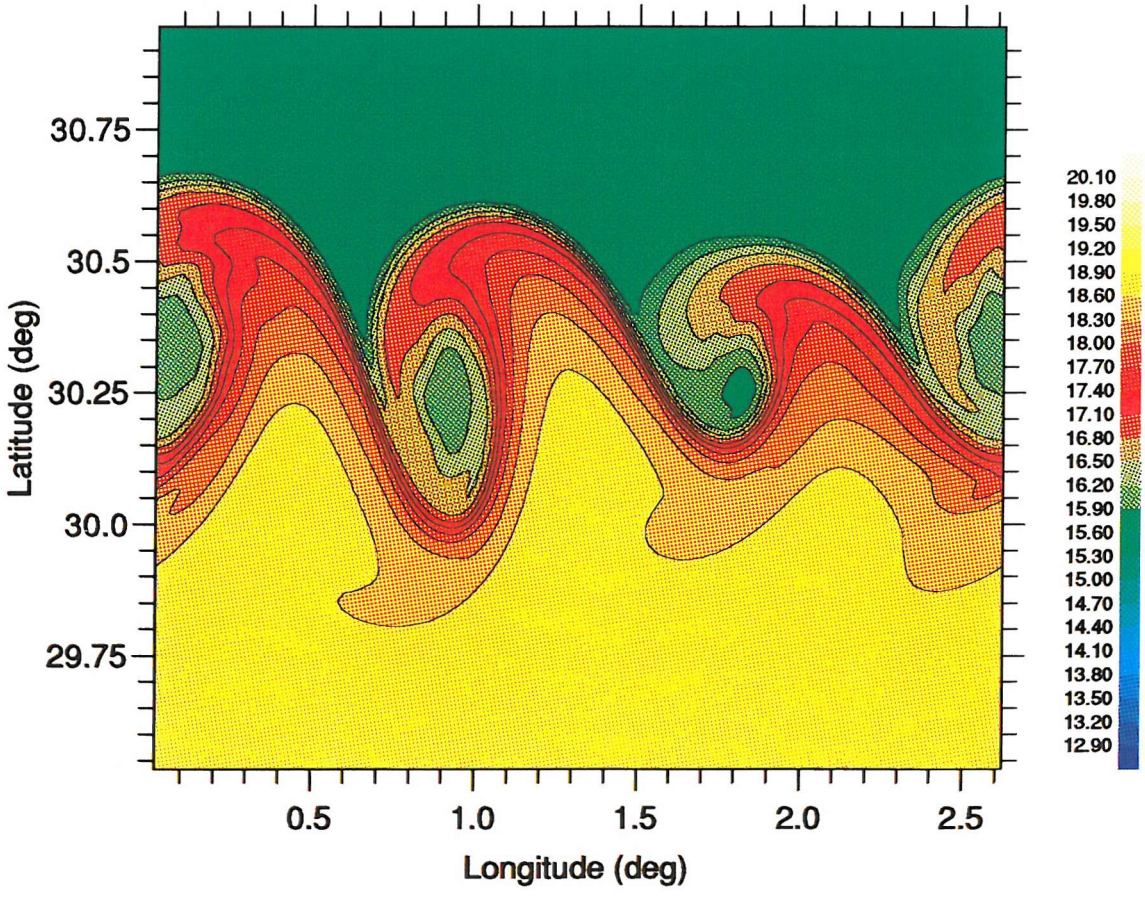

Fig. 5

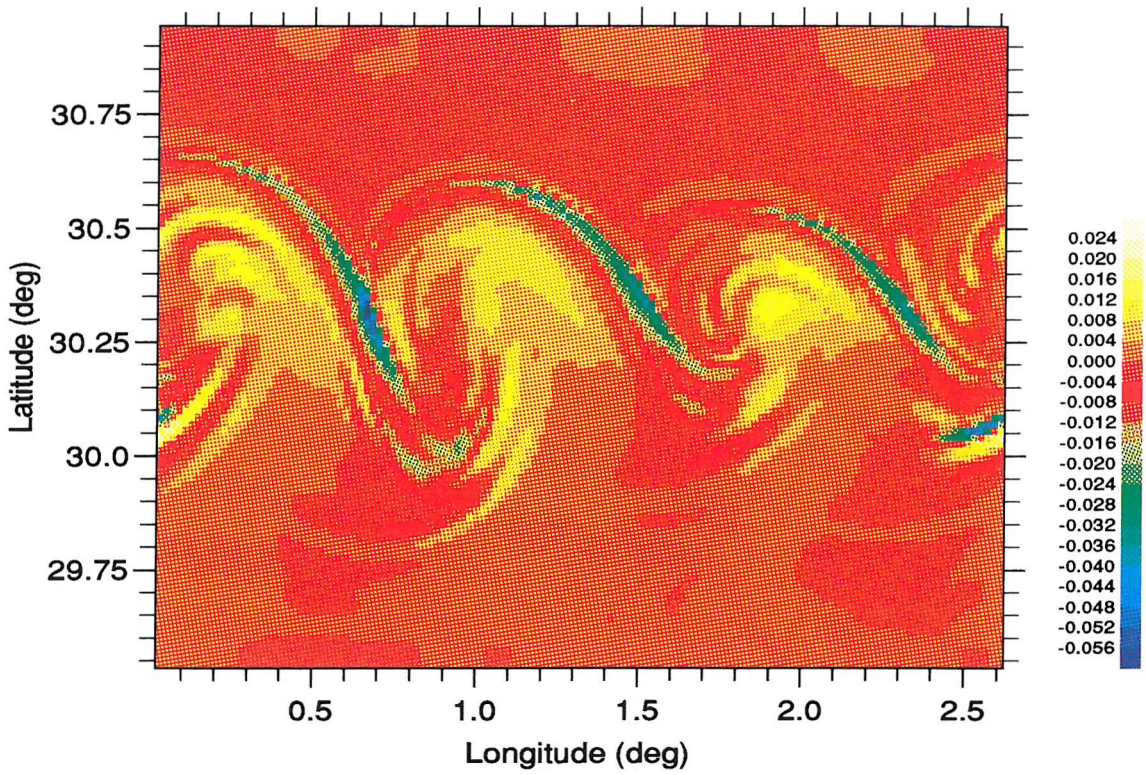
W velocity (cm/s) at depth 30m, min = -0.060, max = 0.024
Latitude (deg)
30.75
30.5
30.25
30.0
29.75
0.5
1.0
1.5
2.0
2.5
Longitude (deg)
0.024
0.020
0.016
0.012
0.008
0.004
0.000
-0.004
-0.008
-0.012
-0.016
-0.020
-0.024
-0.028
-0.032
-0.036
-0.040
-0.044
-0.048
-0.052
-0.056

Fig. 6

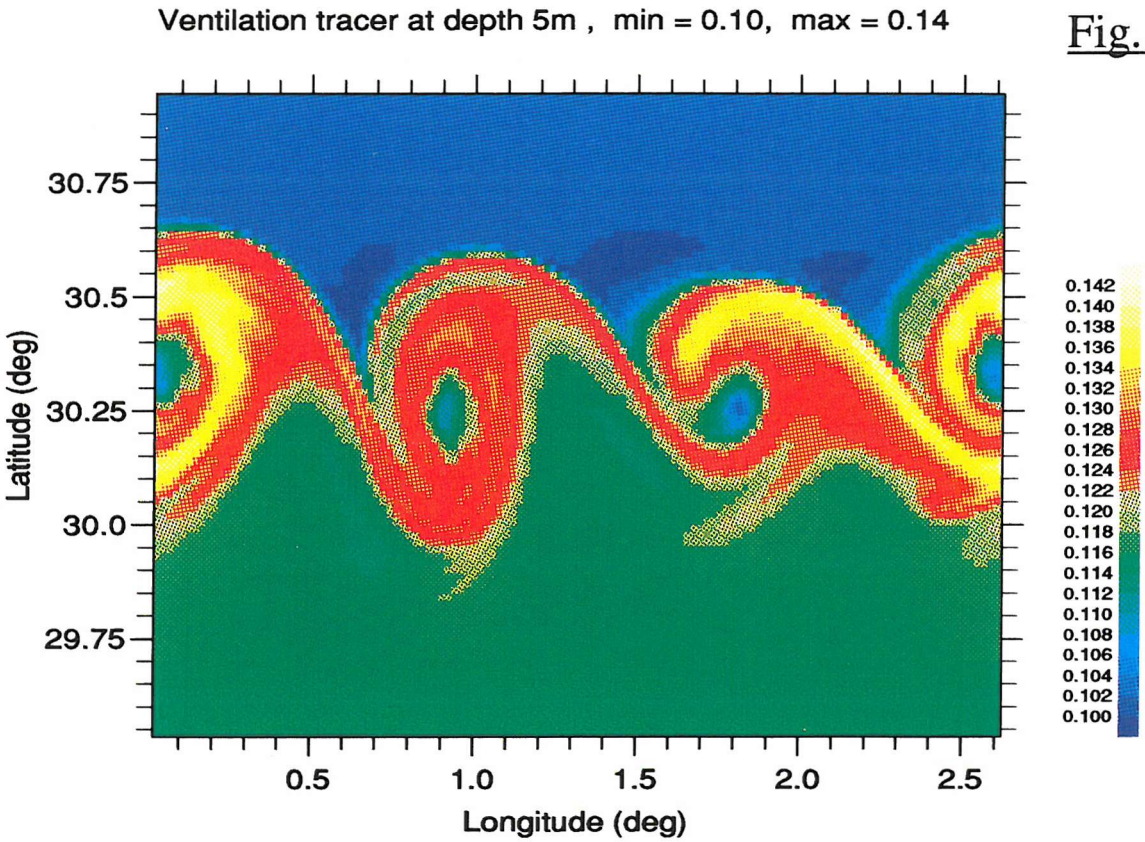
Ventilation tracer at depth 5m , min = 0.10, max = 0.14
Latitude (deg)
30.75
30.5
30.25
30.0
29.75
0.5
1.0
1.5
2.0
2.5
Longitude (deg)
0.142
0.140
0.138
0.136
0.134
0.132
0.130
0.128
0.126
0.124
0.122
0.120
0.118
0.116
0.114
0.112
0.110
0.108
0.106
0.104
0.102
0.100

Mixed-layer Depth (m), C.I = 5.00, min = 10.00, max = 100.00

Fig. 7

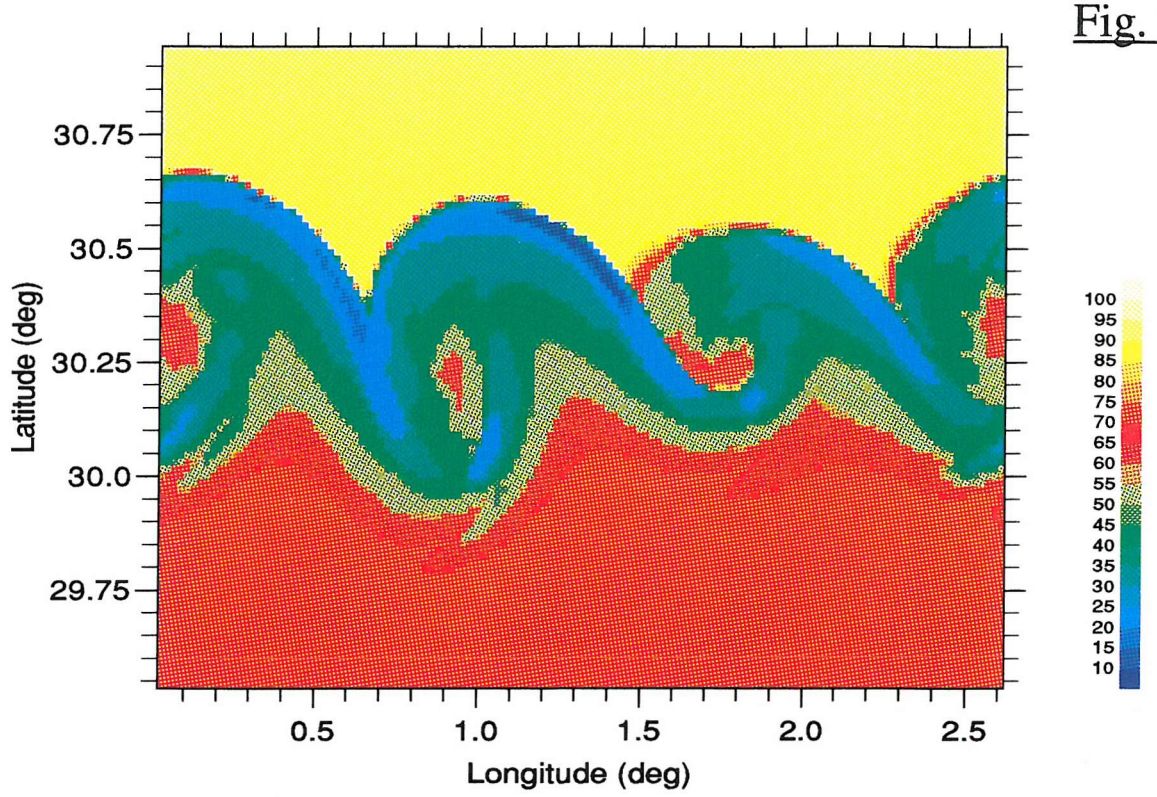

Ventilation tracer at depth 55m, min = 0.00, max = 0.14

Fig. 8

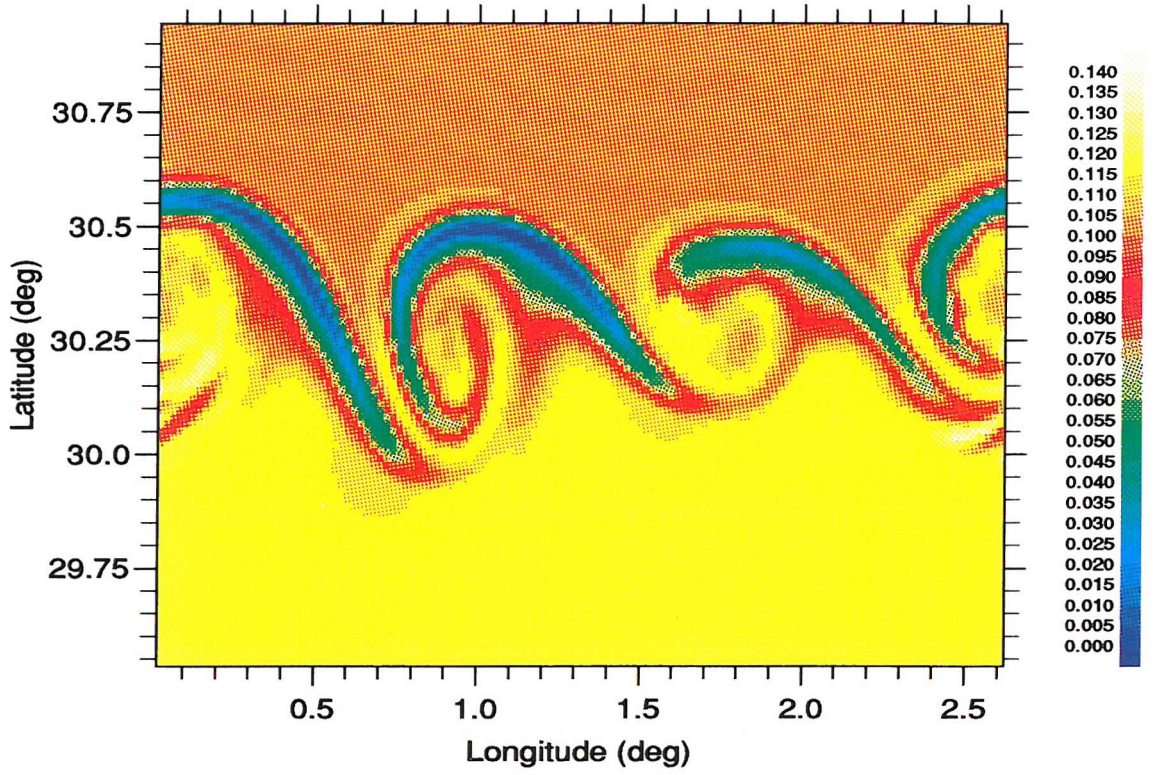

Fig. 9

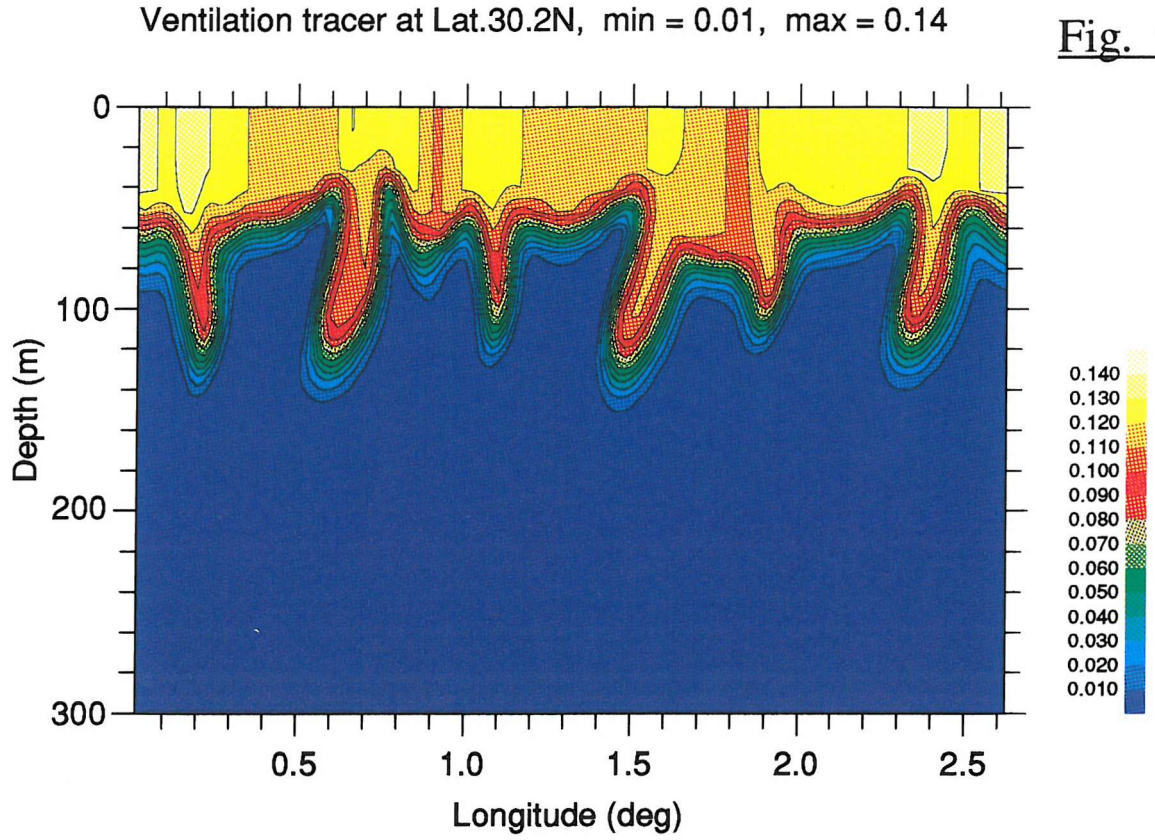
Ventilation tracer at Lat.30.2N, min = 0.01, max = 0.14
Depth (m)
0
100
200
300
0.5
1.0
1.5
2.0
2.5
Longitude (deg)
0.140
0.130
0.120
0.110
0.100
0.090
0.080
0.070
0.060
0.050
0.040
0.030
0.020
0.010

Fig. 10

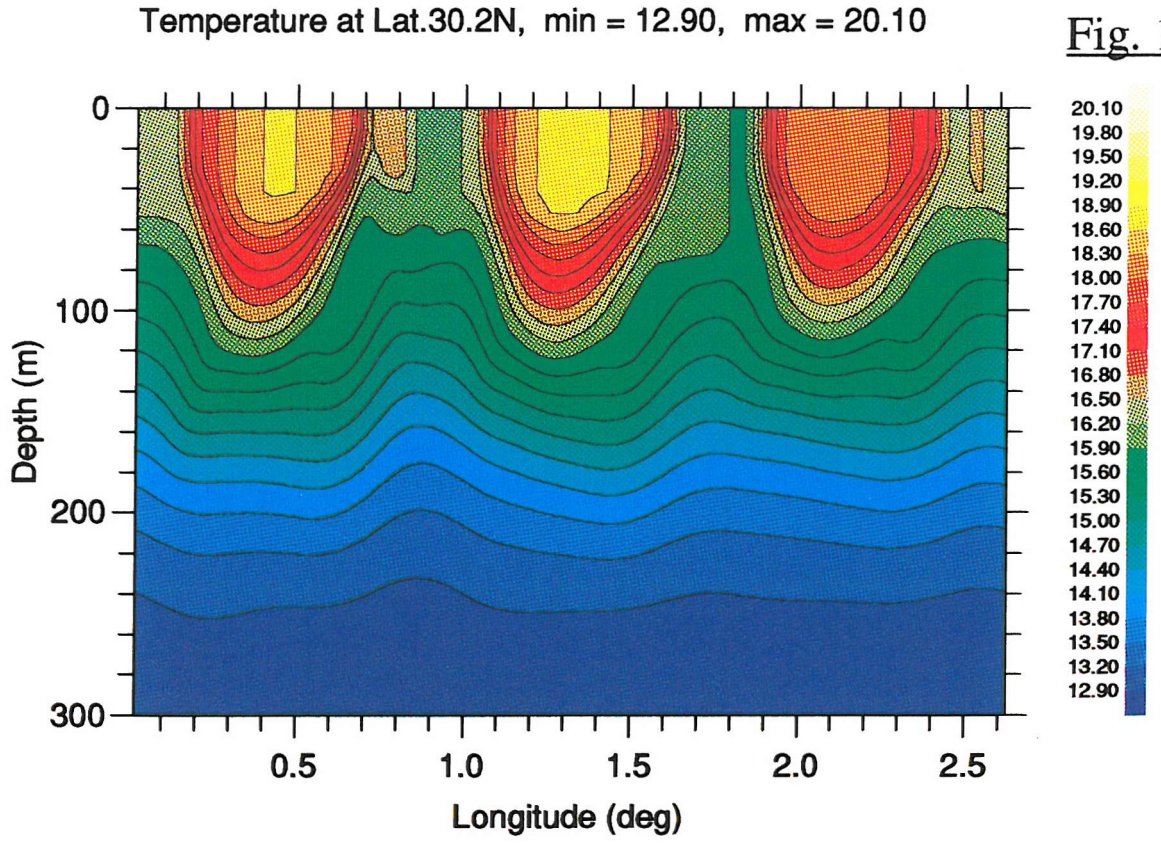
Temperature at Lat.30.2N, min = 12.90, max = 20.10
Depth (m)
0
100
200
300
0.5
1.0
1.5
2.0
2.5
Longitude (deg)
20.10
19.80
19.50
19.20
18.90
18.60
18.30
18.00
17.70
17.40
17.10
16.80
16.50
16.20
15.90
15.60
15.30
15.00
14.70
14.40
14.10
13.80
13.50
13.20
12.90

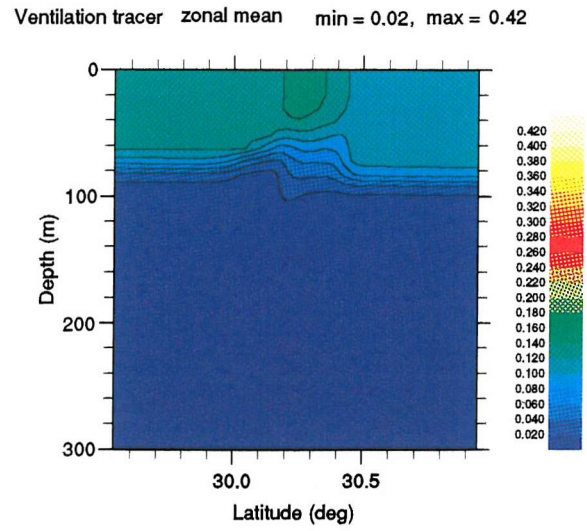

Fig. 11a

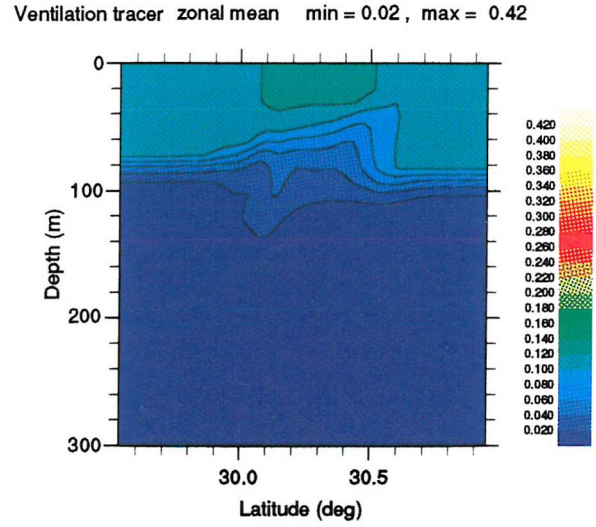

Fig. 11b

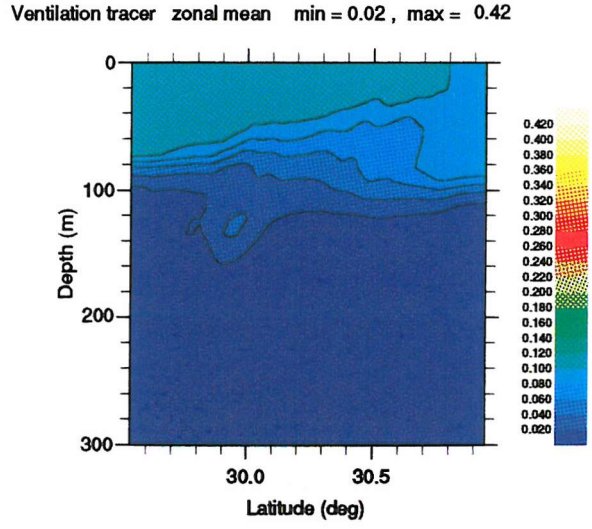

Fig. 11c

Fig. 12

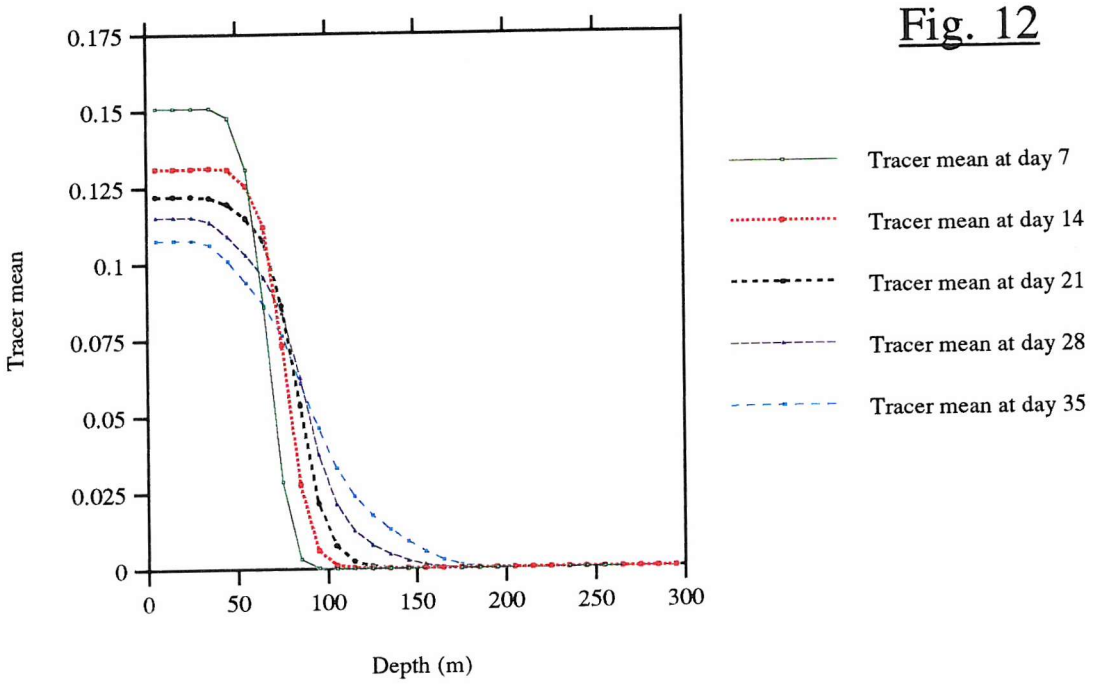
Tracer mean
0.175
0.15
0.125
0.1
0.075
0.05
0.025
0
0
50
100
150
200
250
300
Depth (m)
Tracer mean at day 7
Tracer mean at day 14
Tracer mean at day 21
Tracer mean at day 28
Tracer mean at day 35

Fig. 13

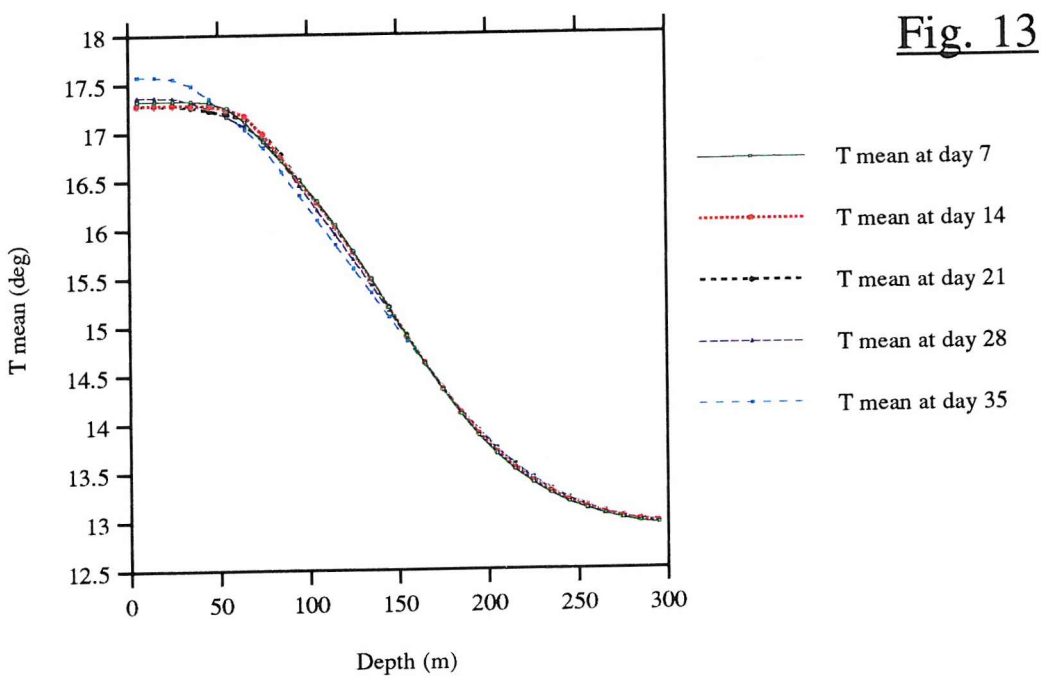
T mean (deg)
18
17.5
17
16.5
16
15.5
15
14.5
14
13.5
13
12.5
0
50
100
150
200
250
300
Depth (m)
T mean at day 7
T mean at day 14
T mean at day 21
T mean at day 28
T mean at day 35

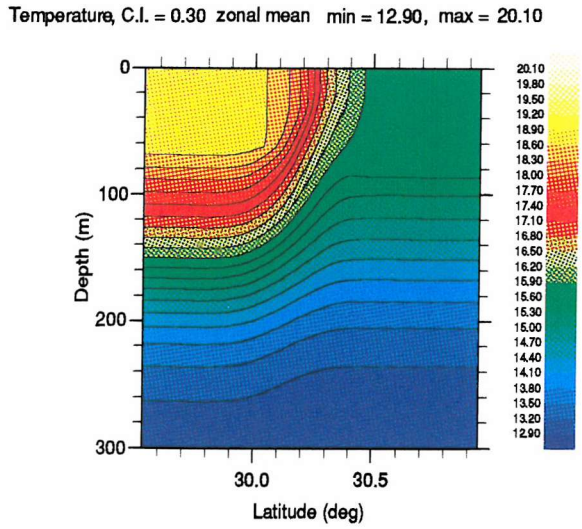

Fig. 14a

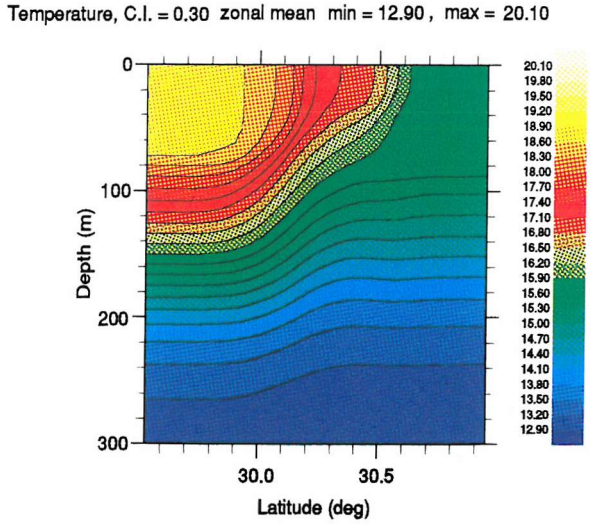

Fig. 14b

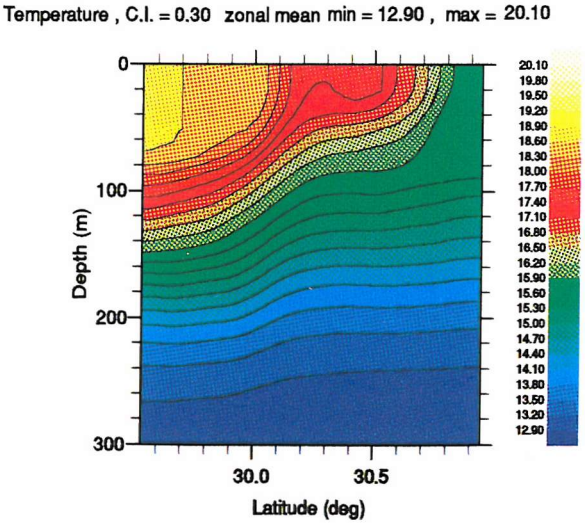

Fig. 14c

Fig. 15

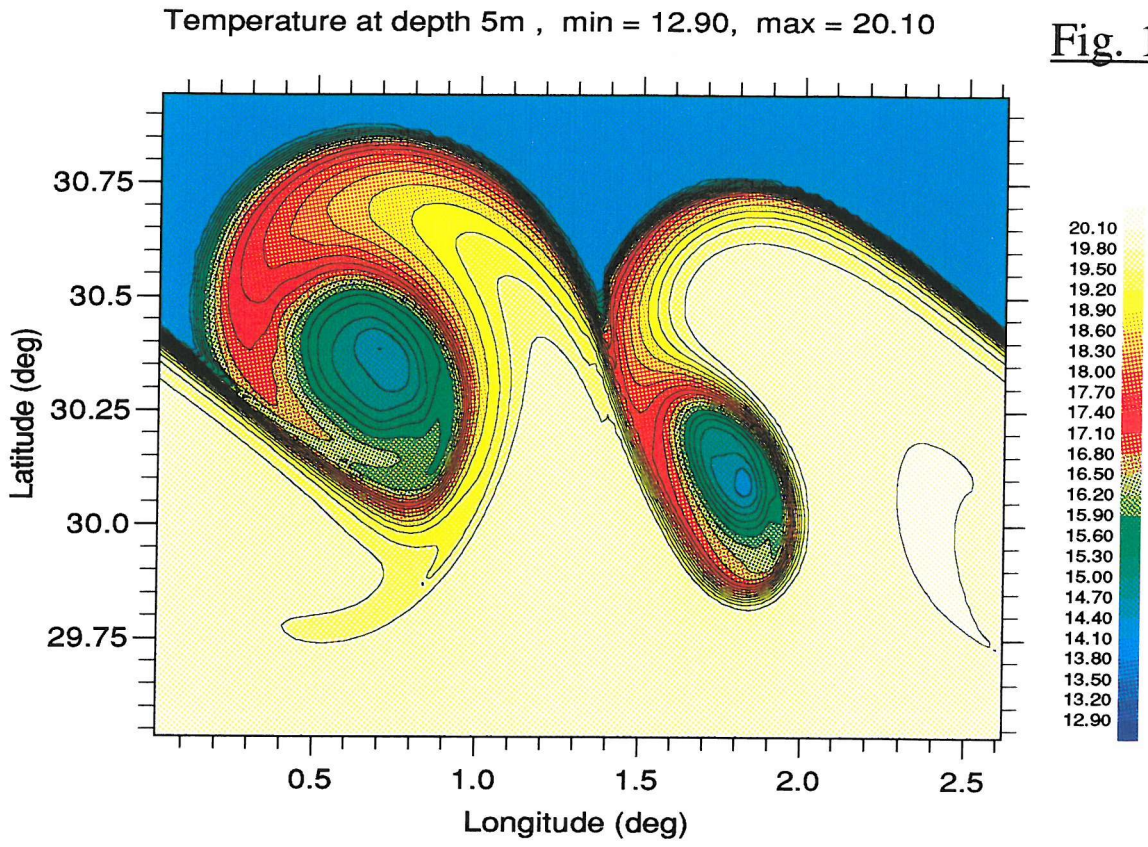
Temperature at depth 5m , min = 12.90, max = 20.10
30.75
30.5
30.25
30.0
29.75
Latitude (deg)
0.5
1.0
1.5
2.0
2.5
Longitude (deg)
20.10
19.80
19.50
19.20
18.90
18.60
18.30
18.00
17.70
17.40
17.10
16.80
16.50
16.20
15.90
15.60
15.30
15.00
14.70
14.40
14.10
13.80
13.50
13.20
12.90

Fig. 16

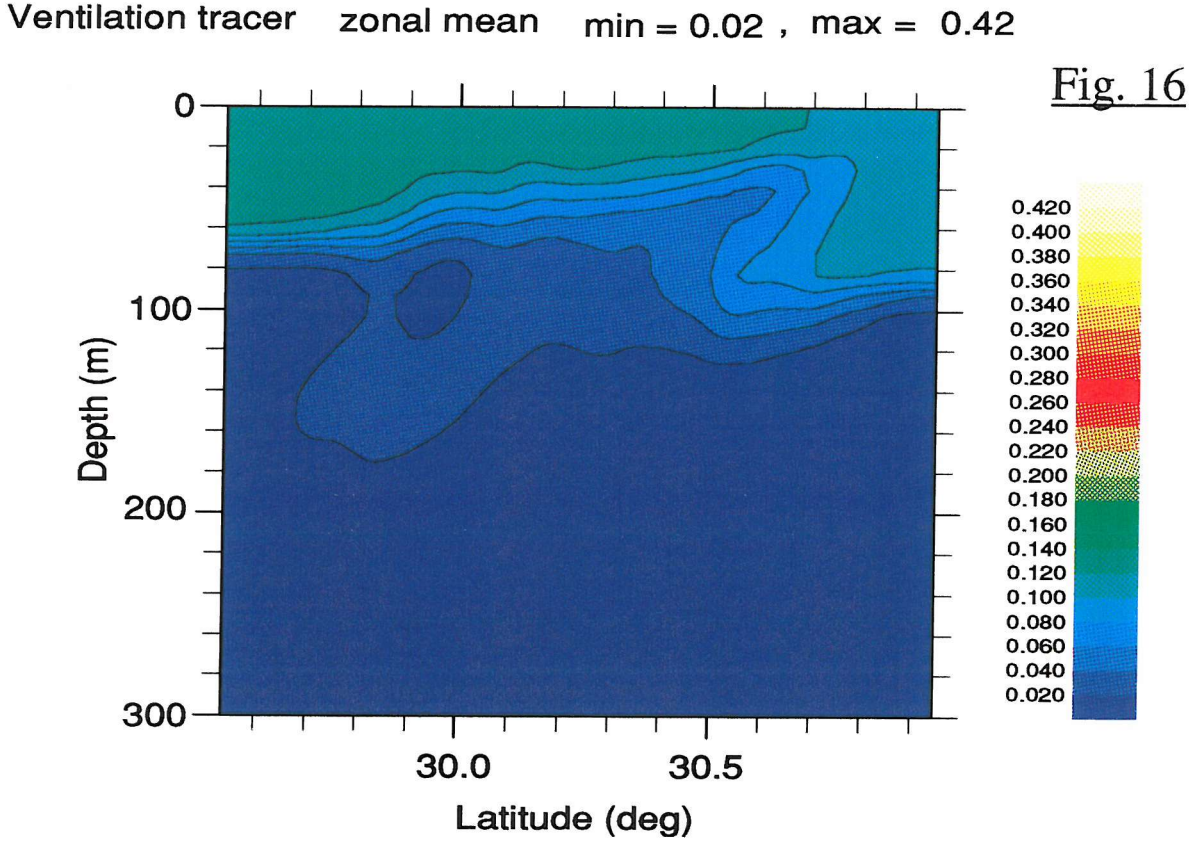
Ventilation tracer zonal mean min = 0.02 , max = 0.42
0
100
200
300
Depth (m)
30.0
30.5
Latitude (deg)
0.420
0.400
0.380
0.360
0.340
0.320
0.300
0.280
0.260
0.240
0.220
0.200
0.180
0.160
0.140
0.120
0.100
0.080
0.060
0.040
0.020

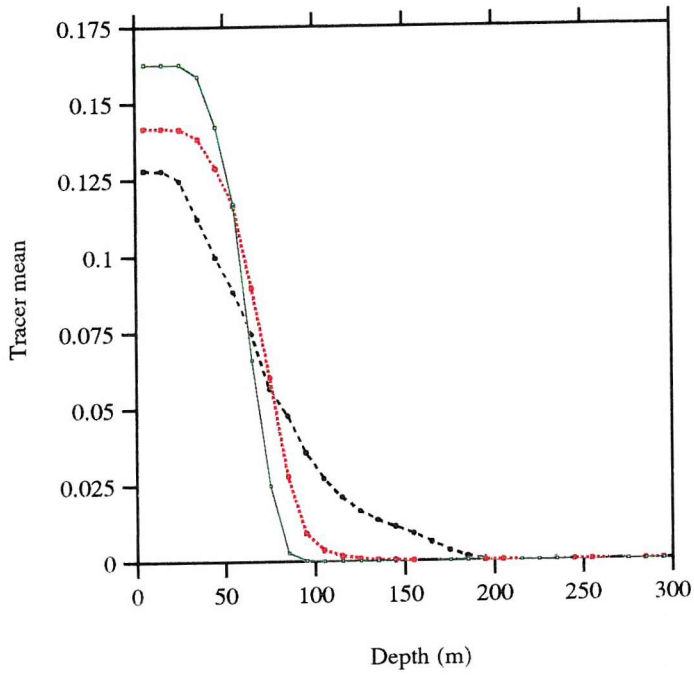
0.175
0.15
0.125
0.1
0.075
0.05
0.025
0
Tracer mean
0
50
100
150
200
250
300
Depth (m)
Tracer mean at day 7
Tracer mean at day 14
Tracer mean at day 21

Fig. 17

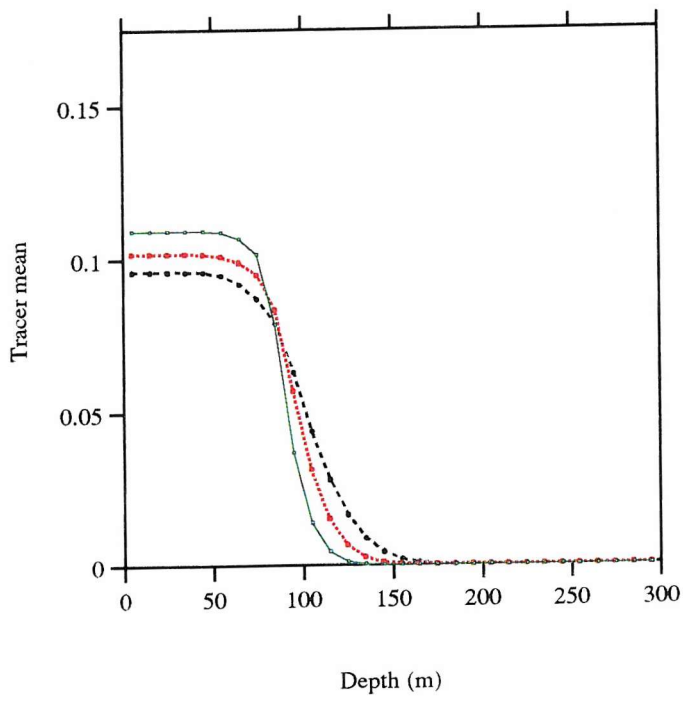
0.15
0.1
0.05
0
Tracer mean
0
50
100
150
200
250
300
Depth (m)
Tracer mean at day 28
Tracer mean at day 42
Tracer mean at day 56

Fig. 18

Fig. 19

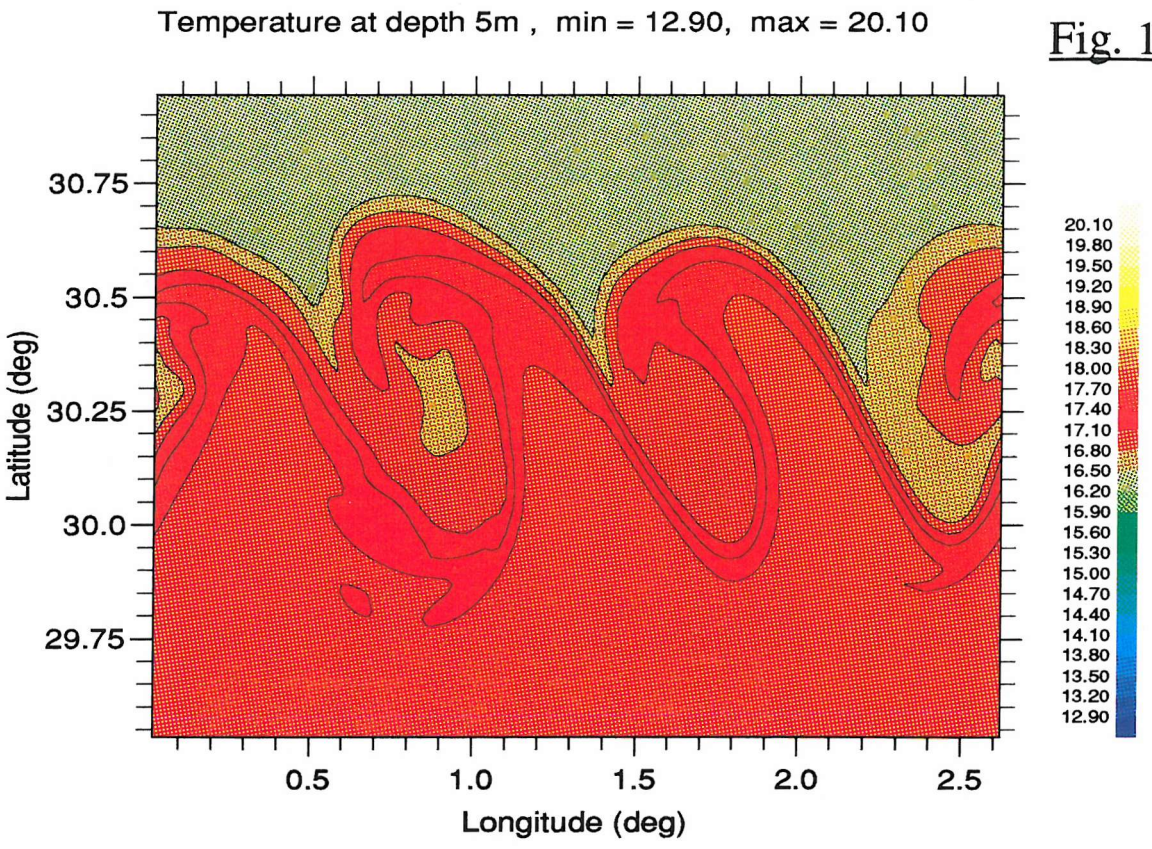
Temperature at depth 5m , min = 12.90, max = 20.10
30.75
30.5
30.25
30.0
29.75
Latitude (deg)
0.5
1.0
1.5
2.0
2.5
Longitude (deg)
20.10
19.80
19.50
19.20
18.90
18.60
18.30
18.00
17.70
17.40
17.10
16.80
16.50
16.20
15.90
15.60
15.30
15.00
14.70
14.40
14.10
13.80
13.50
13.20
12.90

Fig. 20

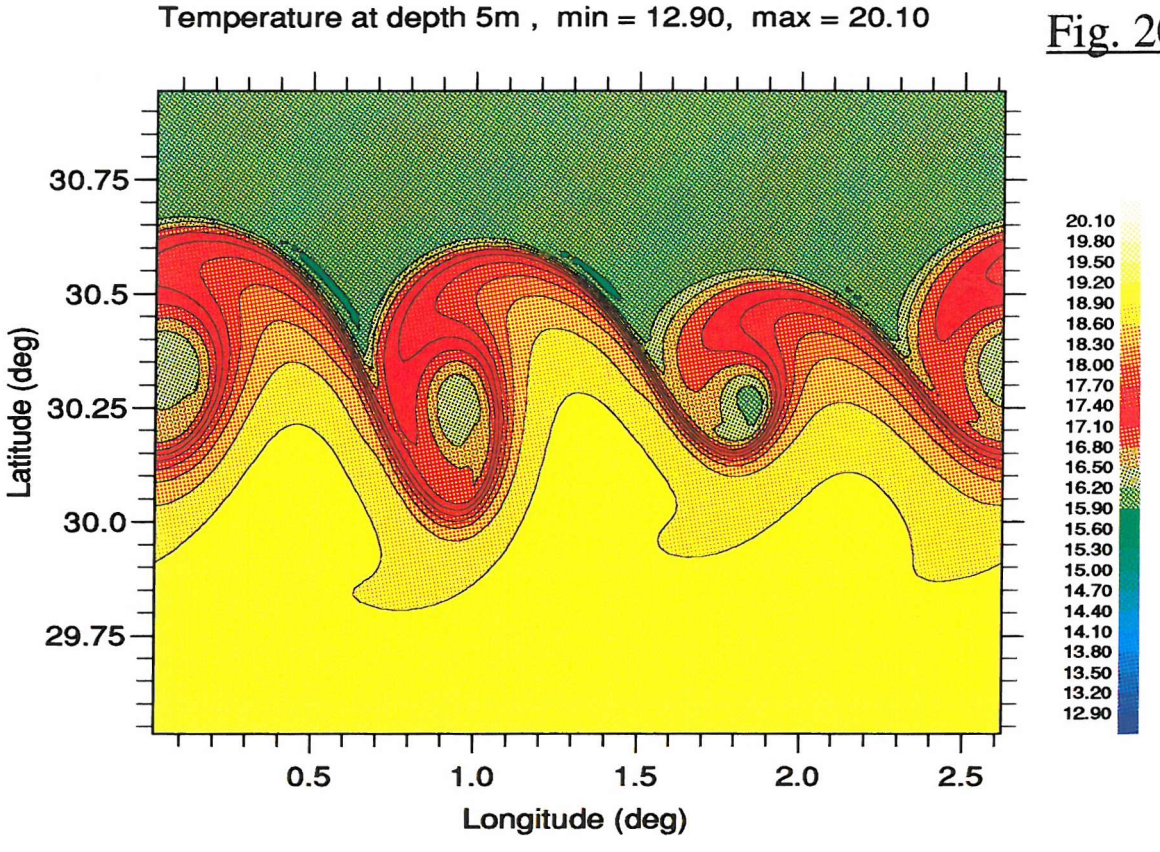
Temperature at depth 5m , min = 12.90, max = 20.10
30.75
30.5
30.25
30.0
29.75
Latitude (deg)
0.5
1.0
1.5
2.0
2.5
Longitude (deg)
20.10
19.80
19.50
19.20
18.90
18.60
18.30
18.00
17.70
17.40
17.10
16.80
16.50
16.20
15.90
15.60
15.30
15.00
14.70
14.40
14.10
13.80
13.50
13.20
12.90

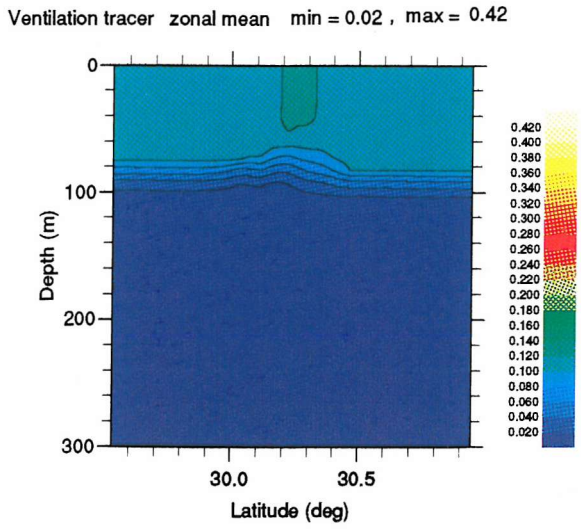

Fig. 21a

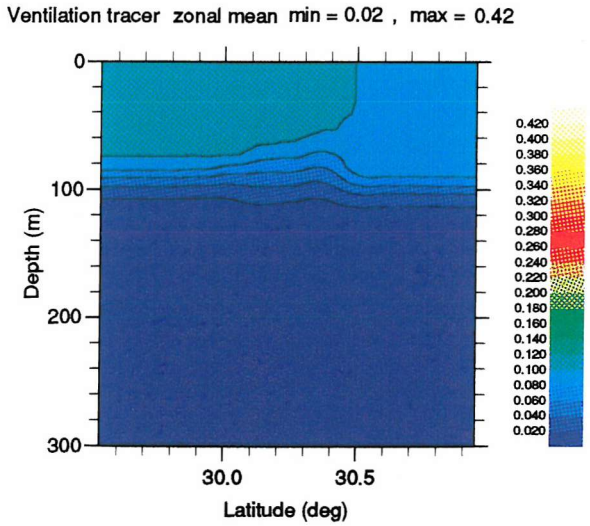

Fig. 21b

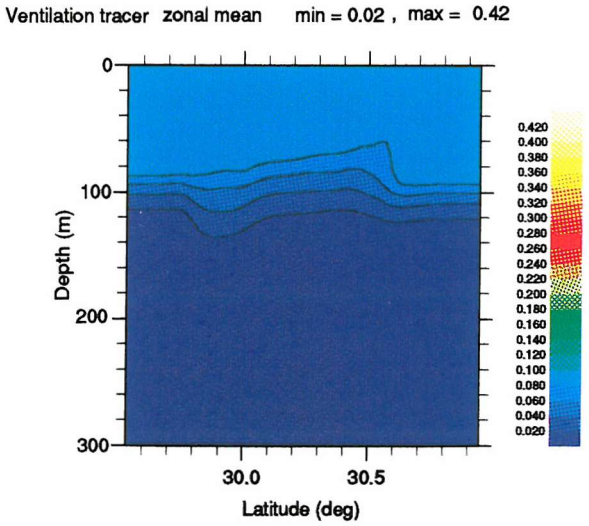

Fig. 21c

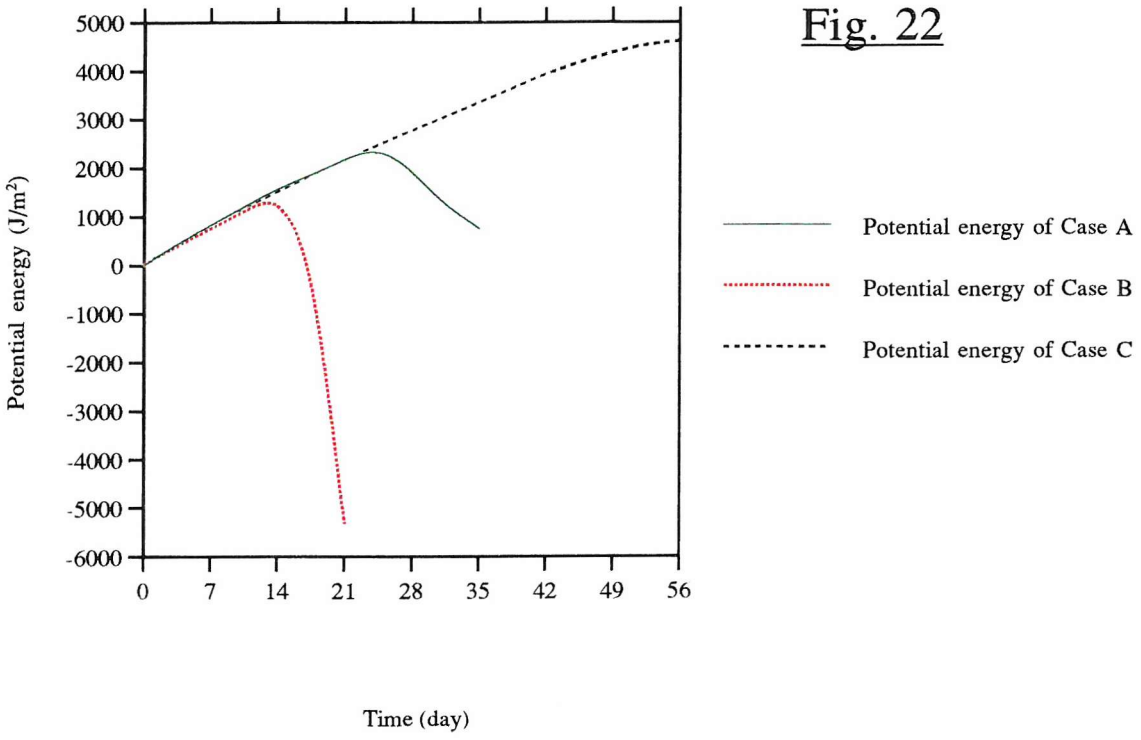
Potential energy (J/m²)
5000
4000
3000
2000
1000
0
-1000
-2000
-3000
-4000
-5000
-6000
0
7
14
21
28
35
42
49
56
Time (day)
Potential energy of Case A
Potential energy of Case B
Potential energy of Case C

Fig. 22

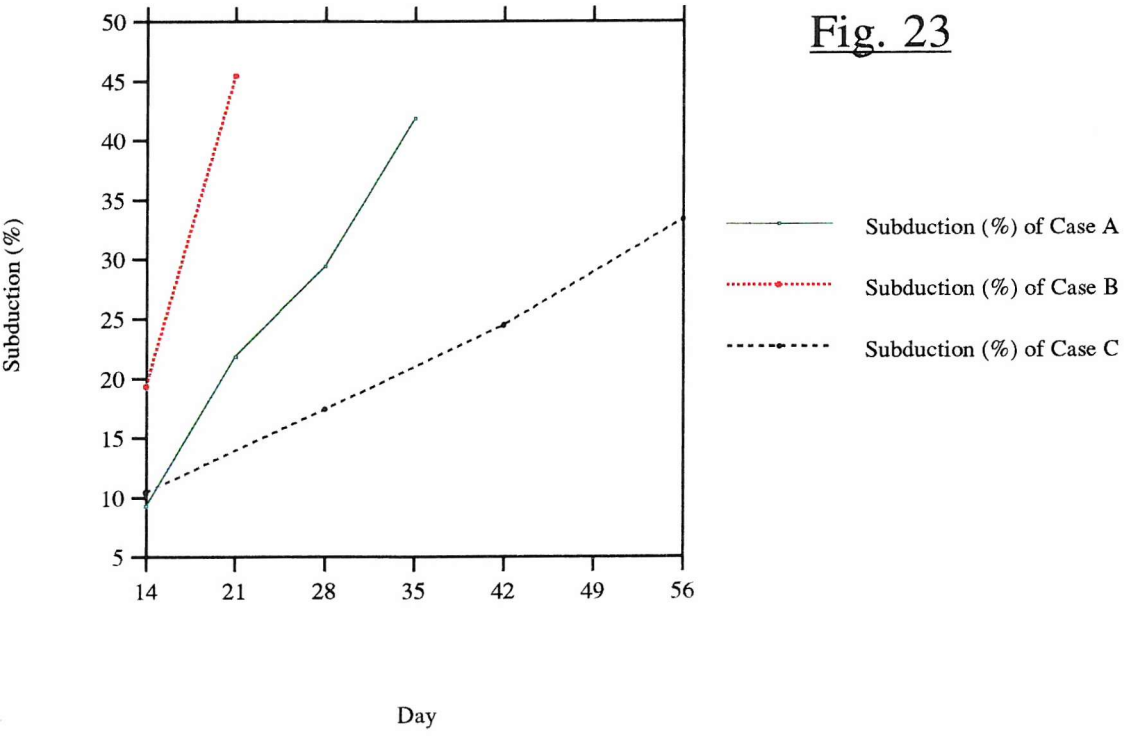
Subduction (%)
50
45
40
35
30
25
20
15
10
5
14
21
28
35
42
49
56
Day
Subduction (%) of Case A
Subduction (%) of Case B
Subduction (%) of Case C

Fig. 23

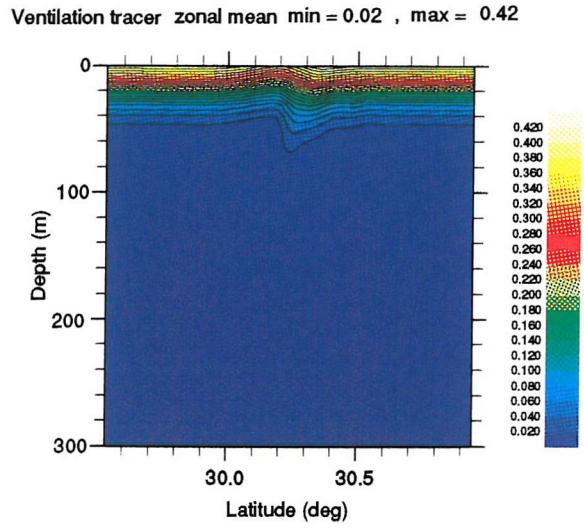

Fig. 24a

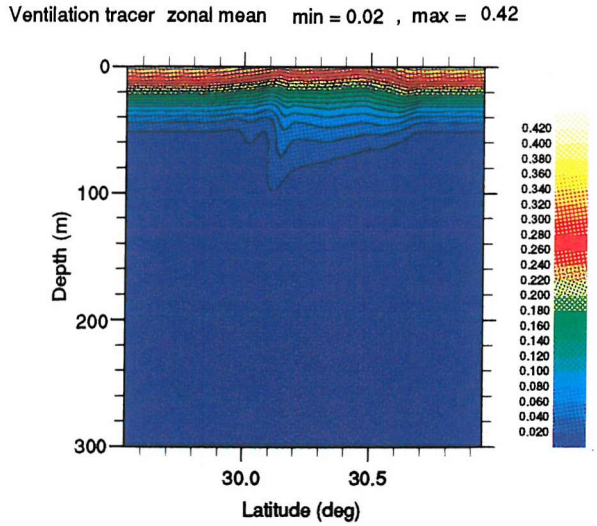

Fig. 24b

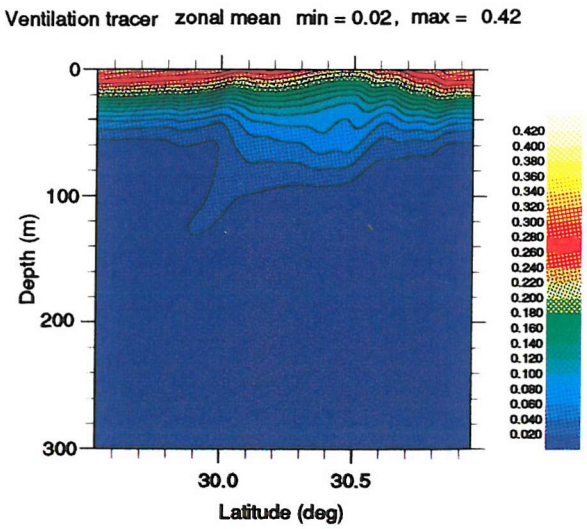

Fig. 24c

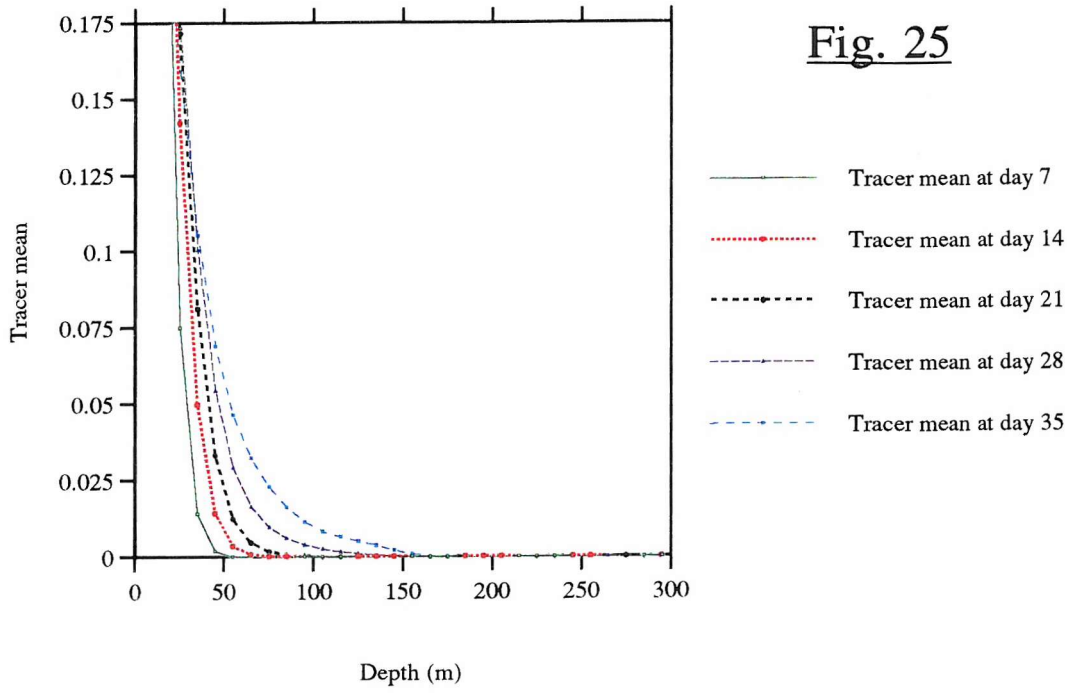
0.175
0.15
0.125
0.1
0.075
0.05
0.025
0
Tracer mean
0
50
100
150
200
250
300
Depth (m)
Tracer mean at day 7
Tracer mean at day 14
Tracer mean at day 21
Tracer mean at day 28
Tracer mean at day 35

Fig. 25

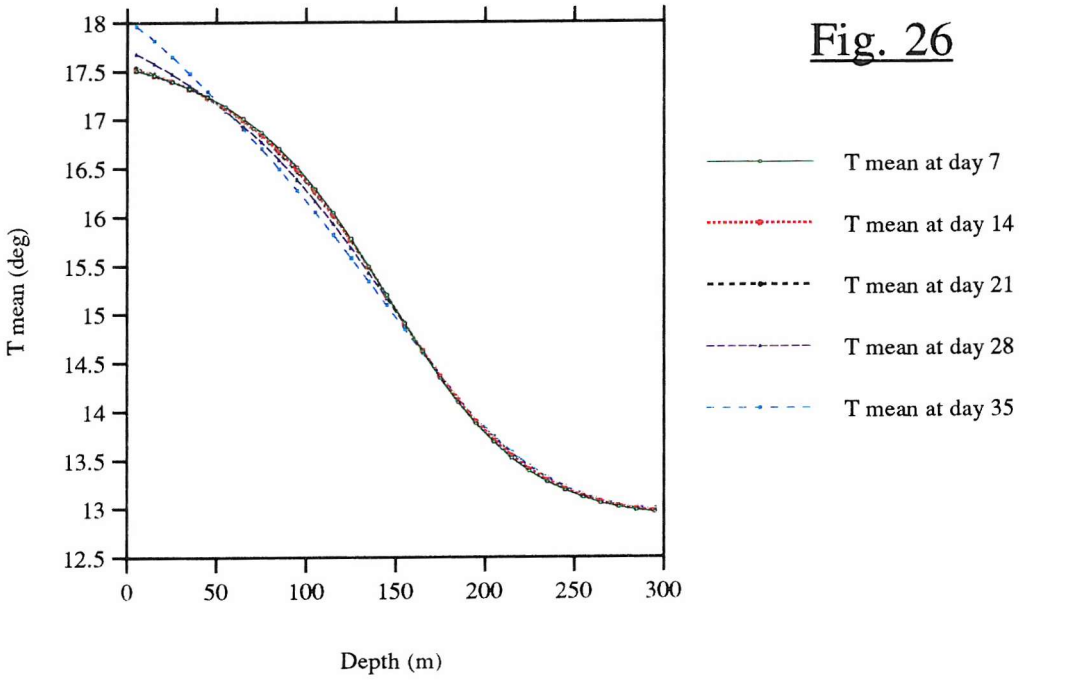
18
17.5
17
16.5
16
15.5
15
14.5
14
13.5
13
12.5
T mean (deg)
0
50
100
150
200
250
300
Depth (m)
T mean at day 7
T mean at day 14
T mean at day 21
T mean at day 28
T mean at day 35

Fig. 26

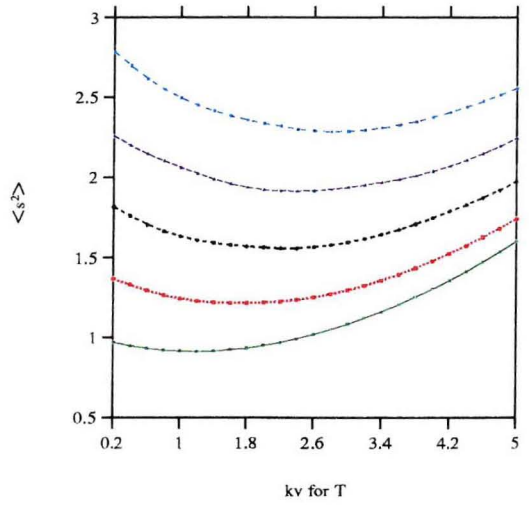

Fig. 27

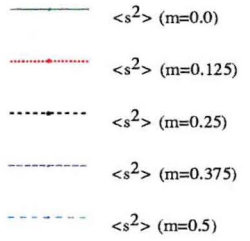

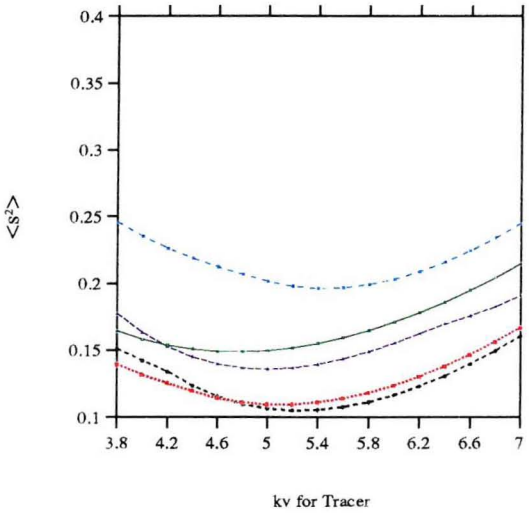

Fig. 28

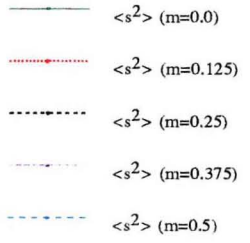

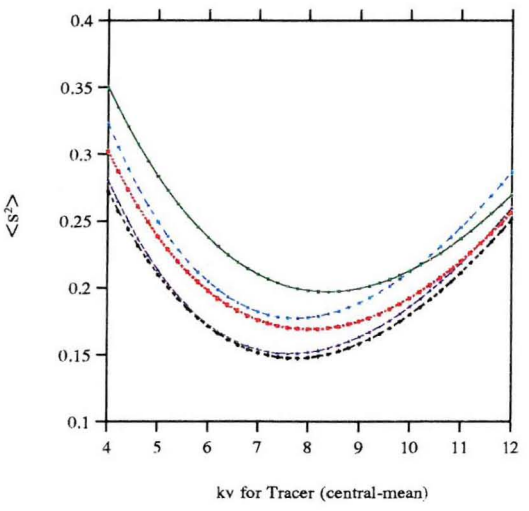

Fig. 29

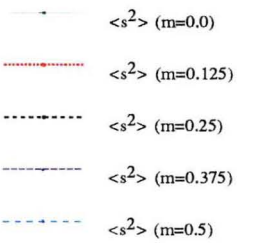

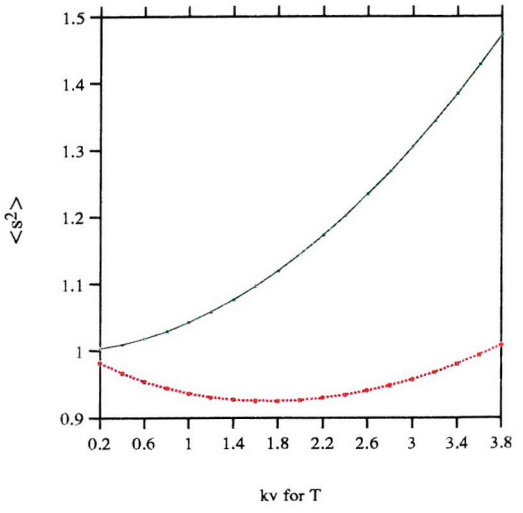
1.5
1.4
1.3
1.2
1.1
1
0.9
<s2>
0.2 0.6 1 1.4 1.8 2.2 2.6 3 3.4 3.8
kv for T

Fig. 30

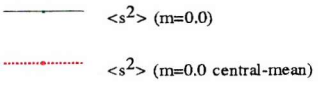
<s2> (m=0.0)
<s2> (m=0.0 central-mean)

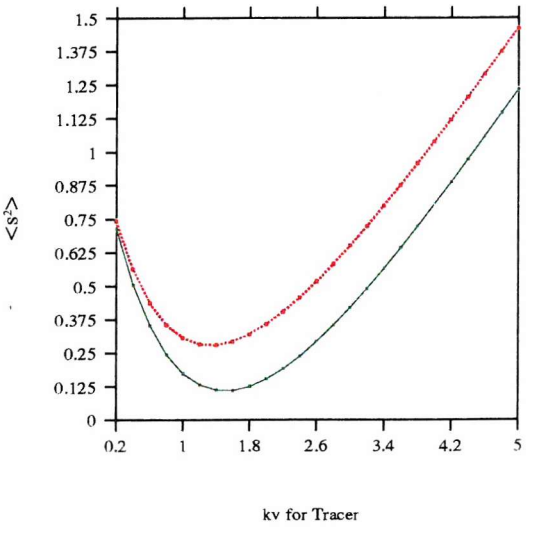
1.5
1.375
1.25
1.125
1
0.875
0.75
0.625
0.5
0.375
0.25
0.125
0
<s2>
0.2 1 1.8 2.6 3.4 4.2 5
kv for Tracer

Fig. 31

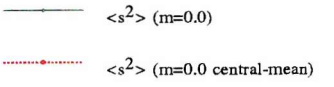
<s2> (m=0.0)
<s2> (m=0.0 central-mean)

Fig. 32

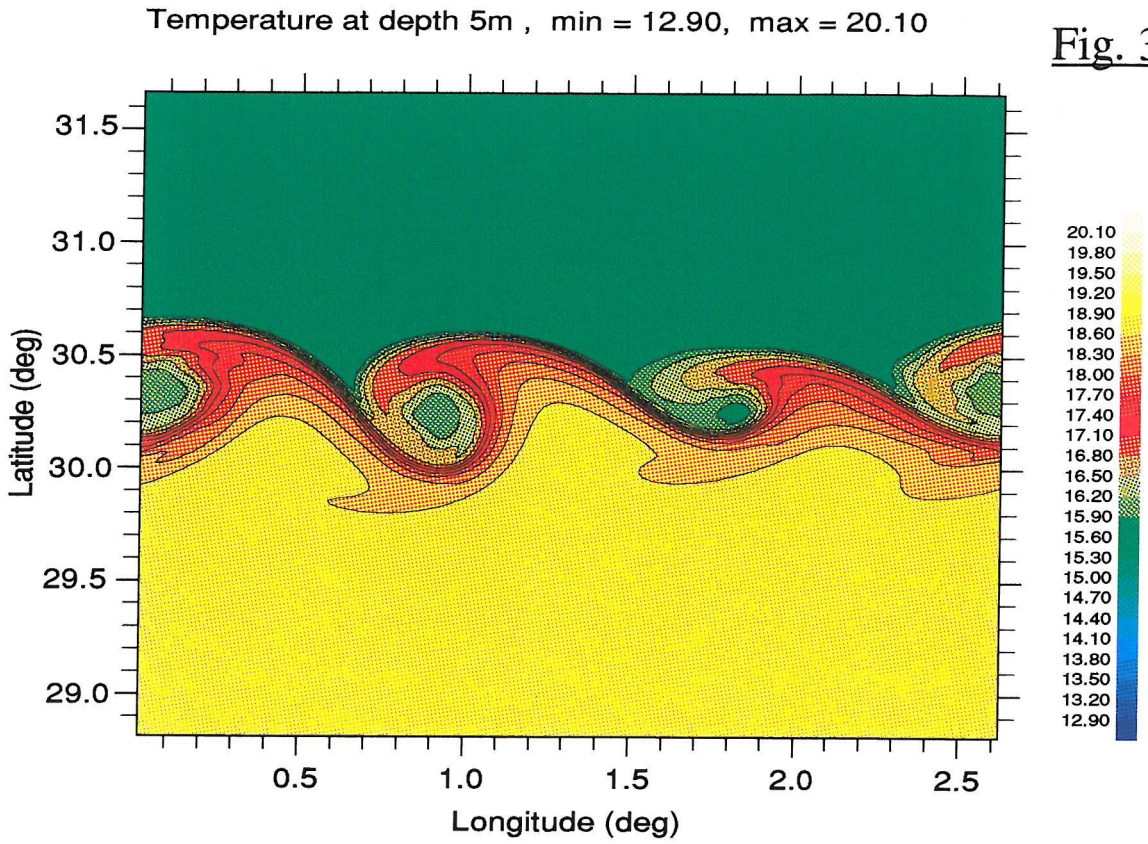
Temperature at depth 5m , min = 12.90, max = 20.10
Latitude (deg)
31.5
31.0
30.5
30.0
29.5
29.0
0.5
1.0
1.5
2.0
2.5
Longitude (deg)
20.10
19.80
19.50
19.20
18.90
18.60
18.30
18.00
17.70
17.40
17.10
16.80
16.50
16.20
15.90
15.60
15.30
15.00
14.70
14.40
14.10
13.80
13.50
13.20
12.90

Fig. 33

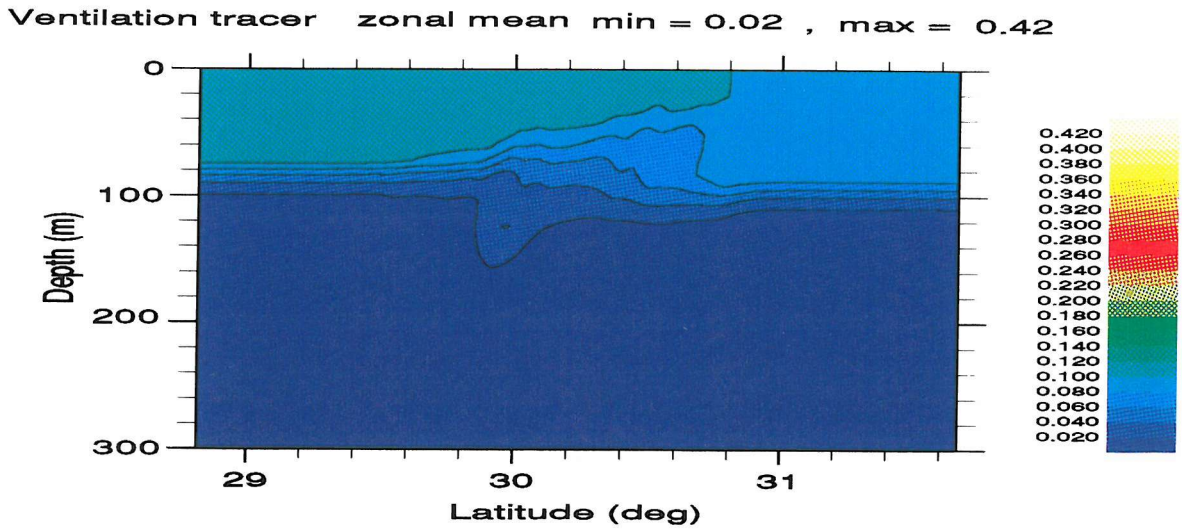
Ventilation tracer zonal mean min = 0.02 , max = 0.42
Depth (m)
0
100
200
300
29
30
31
Latitude (deg)
0.420
0.400
0.380
0.360
0.340
0.320
0.300
0.280
0.260
0.240
0.220
0.200
0.180
0.160
0.140
0.120
0.100
0.080
0.060
0.040
0.020

Fig. 34

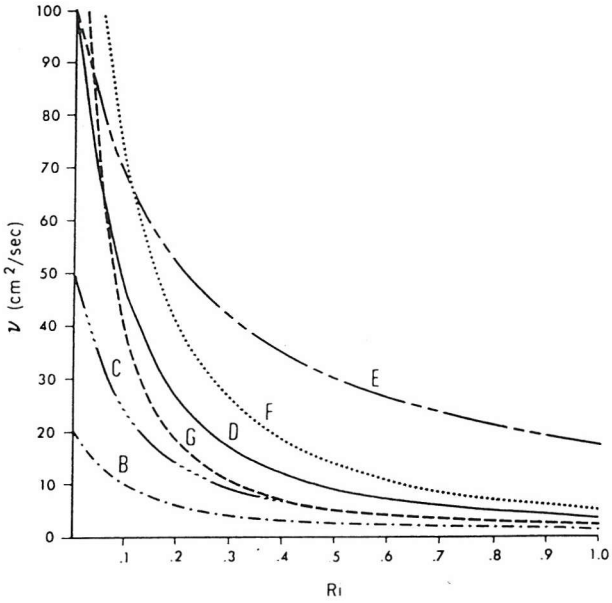
100
90
80
70
60
50
40
30
20
10
0
ν (cm²/sec)
.1
.2
.3
.4
.5
.6
.7
.8
.9
1.0
Ri
B
C
D
E
F
G

Fig. 35

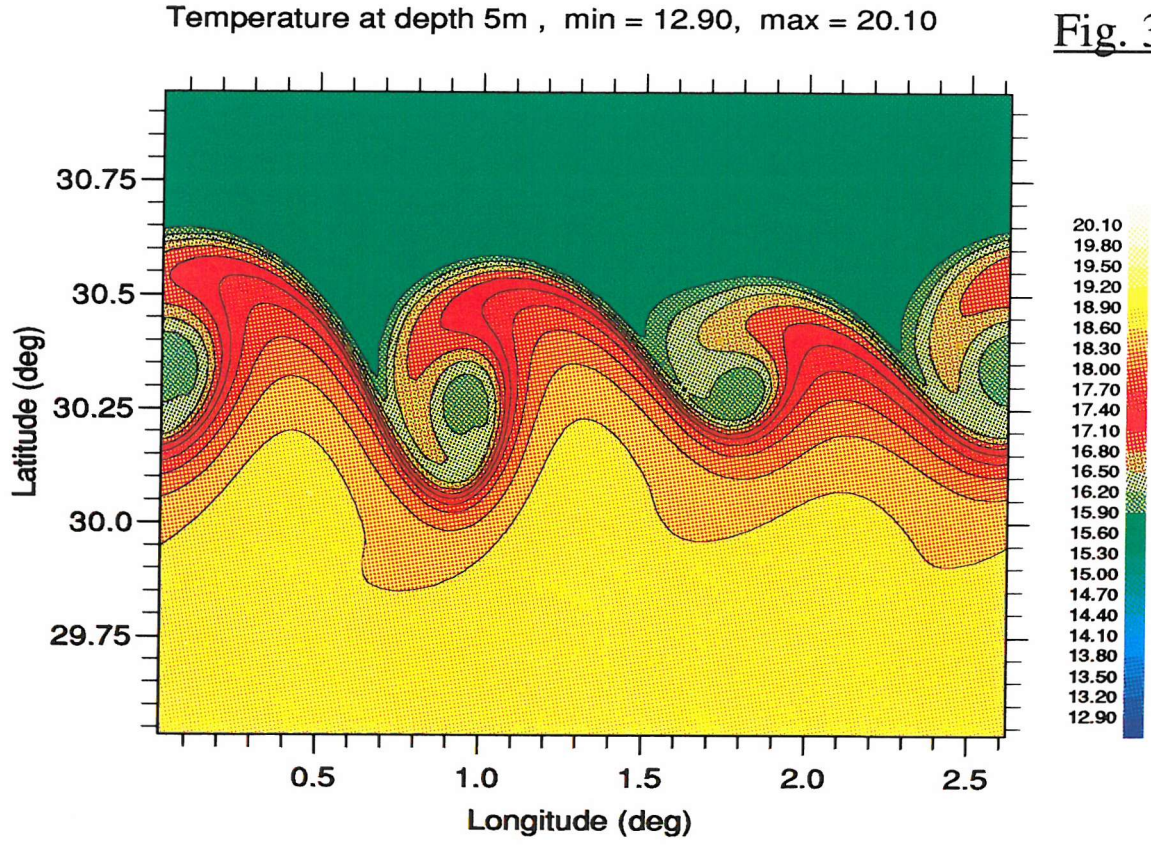
Temperature at depth 5m , min = 12.90, max = 20.10
30.75
30.5
30.25
30.0
29.75
Latitude (deg)
0.5
1.0
1.5
2.0
2.5
Longitude (deg)
20.10
19.80
19.50
19.20
18.90
18.60
18.30
18.00
17.70
17.40
17.10
16.80
16.50
16.20
15.90
15.60
15.30
15.00
14.70
14.40
14.10
13.80
13.50
13.20
12.90

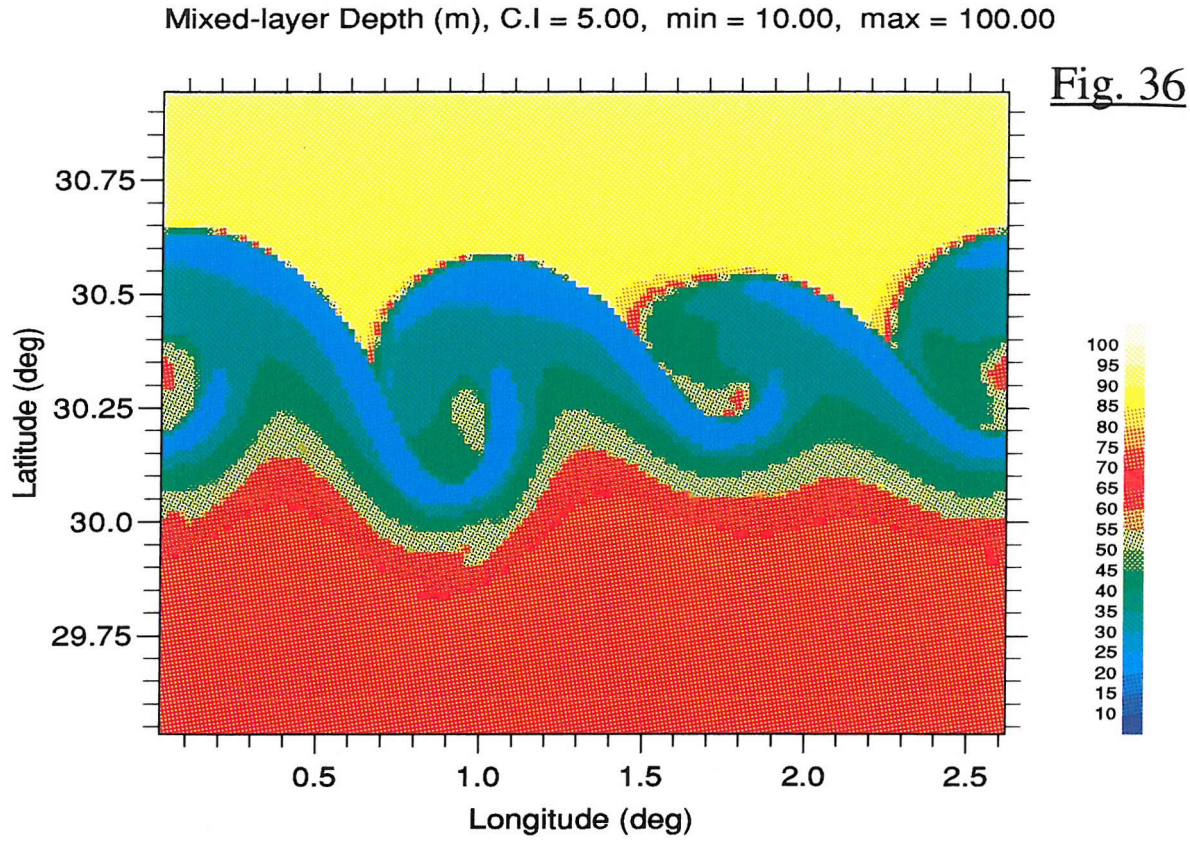
Mixed-layer Depth (m), C.I = 5.00, min = 10.00, max = 100.00
30.75
30.5
30.25
30.0
29.75
Latitude (deg)
0.5
1.0
1.5
2.0
2.5
Longitude (deg)
100
95
90
85
80
75
70
65
60
55
50
45
40
35
30
25
20
15
10

Fig. 36

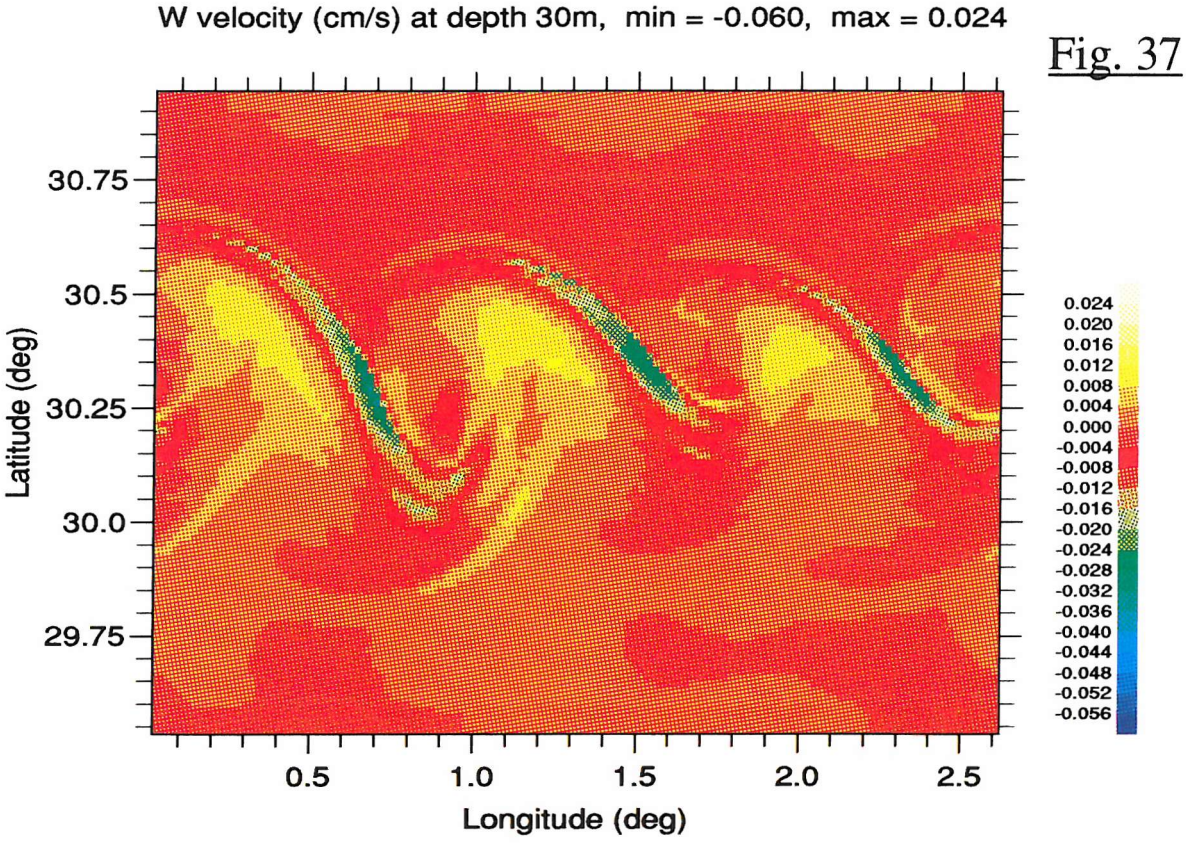
W velocity (cm/s) at depth 30m, min = -0.060, max = 0.024
30.75
30.5
30.25
30.0
29.75
Latitude (deg)
0.5
1.0
1.5
2.0
2.5
Longitude (deg)
0.024
0.020
0.016
0.012
0.008
0.004
0.000
-0.004
-0.008
-0.012
-0.016
-0.020
-0.024
-0.028
-0.032
-0.036
-0.040
-0.044
-0.048
-0.052
-0.056

Fig. 37

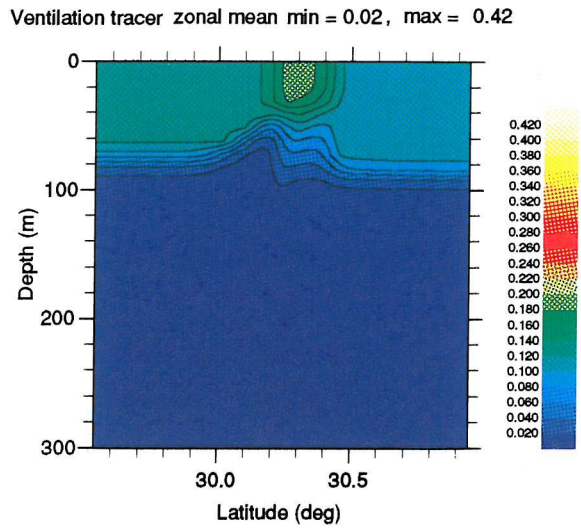

Fig. 38a

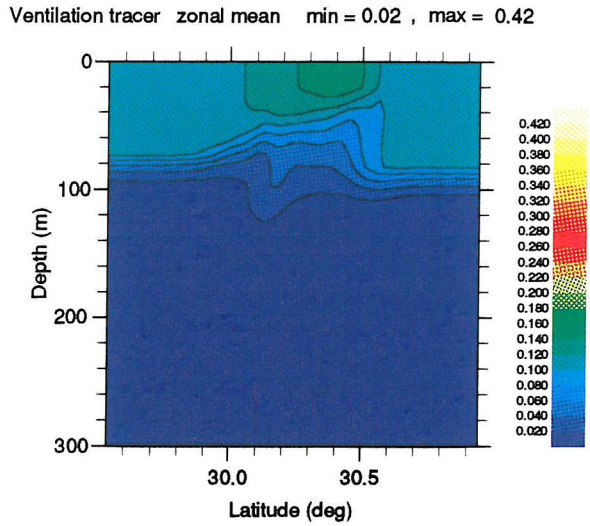

Fig. 38b

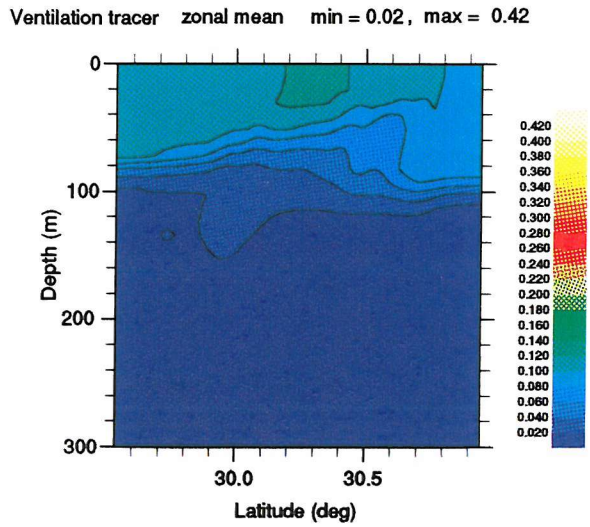

Fig. 38c

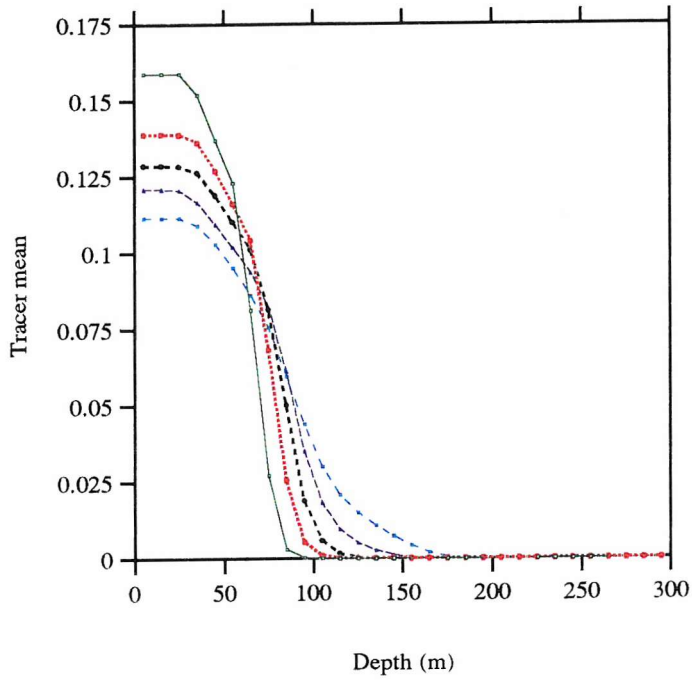

Fig. 39

Tracer mean at day 7
Tracer mean at day 14
Tracer mean at day 21
Tracer mean at day 28
Tracer mean at day 35

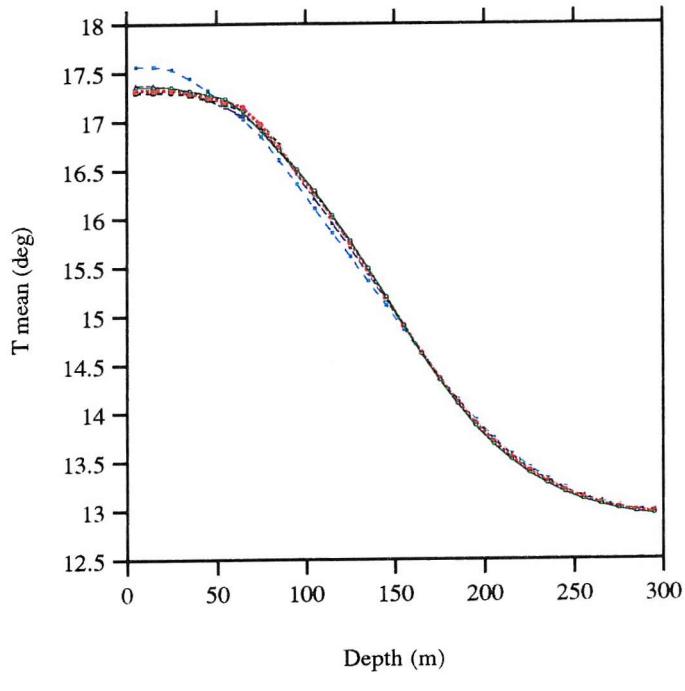

Fig. 40

T mean at day 7
T mean at day 14
T mean at day 21
T mean at day 28
T mean at day 35


Natural
Environment
Research
Council